CHAPTER 1

INTRODUCTION

α-Amylases are among the most important enzymes and of great significance in present day biotechnology. They are used for production of maltodextrins to make high fructose corn syrup, baking, brewing, alcohol, detergent and textile industries (Pandey et al., 2000; Ammar et al., 2002; Varavinita et al., 2002; Bessler et al., 2003; Nagarajan et al., 2006). Due to the high thermostability (T_m ~ 103°C) of *Bacillus licheniformis* α-amylase (BLA) (Fitter & Haber-Pohlmeier, 2004), it has become the enzyme of choice in starch processing industry which requires high temperature operations (Vihinen & Mäntsälä, 1989; Janeček & Baláž, 1992). Being a thermophilic enzyme from a mesophilic organism (Duy & Fitter, 2005), BLA has attracted the attention of many researchers to study structure-function relationship of this enzyme (Tomazic & Klibanov, 1988; Machius et al., 1995; Khajeh et al., 2001a; Khajeh et al., 2001b; Fitter & Haber-Pohlmeier, 2004; Nazmi et al., 2006). In fact, BLA is even more stable than its homologous counterparts (Declerck et al., 2002). Considering the high homology in primary and tertiary structures with other α-amylases from *Bacillus sp. e.g. Bacillus amyloliquefaciens* α-amylase (BAA) and *Bacillus stearothermophilus* α-amylase (BStA), BLA possesses a much higher half-life than others under similar conditions (Table 1.1) (Tomazic & Klibanov, 1988). Comparative studies on BAA and BLA have revealed that a few salt bridges in BLA (which were absent in BAA) could be responsible for its enhanced thermostability (Tomazic & Klibanov, 1988; Machius et al., 1995). Specifically, presence of five lysine residues at positions of 88, 253, 308, 317 and 385 in the non-homologous regions of the primary sequence of BLA seems to offer greater thermostability to the enzyme (Tomazic & Klibanov, 1988). Furthermore, substitutions of lysine residues at positions 88, 253 and 385 of BLA with uncharged residues (glycine, alanine and asparagine) have been shown to decrease the

Table 1.1: Properties of several α-amylases from *Bacillus sp.*.[*]

Source	***Bacillus licheniformis***	***Bacillus amyloliquefaciens***	***Bacillus stearothermophilus***
No. of residues	483	483	515
Identity with BLA (%)	100	81	64
Half-life ($T_{1/2}$, min)[#]	270	2	50

[#]Half-life of these enzymes was determined at 90°C, pH 6.5 (Tomazic & Klibanov, 1988).

[*]With kind permission from Springer Science + Business Media: <Biologia Bratislavia, Engineering the thermostability of *Bacillus licheniformis* α-amylase, 57, 2002, 203–211, Declerck, N., Machius, M., Joyet, P., Wiegand, G., Huber, R., & Gaillardin, C., Table 1).

thermostability of the enzyme, suggesting the role of lysine residues in increasing the thermostability of BLA through salt bridges (Tomazic & Klibanov, 1988). Another common requirement for the enhanced thermal stability of BLA is the presence of calcium in its calcium binding sites (Vihinen & Mäntsälä, 1989; Violet & Meunier, 1989; Feller et al., 1999). Since thermostable proteins have also been found resistant towards chemical denaturation (Griffin et al., 2003), it would be of interest to study the role of electrostatic interactions (salt bridges) in the conformational stability of the enzyme against chemical denaturants. Chemical modification would be a useful approach to study the role of salt bridges in the conformational stability of BLA. Hence, following objectives were set forth in this study.

i. To study the role of electrostatic interactions in the conformational stability of BLA;
ii. To compare the effect of calcium on the stability of BLA against urea and GdnHCl denaturation.

CHAPTER 2

LITERATURE REVIEW

2.1 Background

In order to perform their biological functions, proteins fold into a specific three-dimensional conformation, driven by non-covalent forces such as hydrogen bonds, hydrophobic packing, van der Waals and electrostatic interactions as well as covalent bonds (disulfide bridges), if present (Anfinsen, 1973). Although most proteins are mainly stabilized by hydrophobic packing and hydrogen bonds (Machius et al., 2003; Pace, 2009), electrostatic interactions between charged residues do contribute significantly towards maintaining the native three-dimensional structure of a protein (Serrano et al., 1990; Singh & Bhakuni, 2008). These charged residues (~23% of the total number of amino acid residues in proteins) are mostly distributed at the protein's surface (Miller et al., 1987; Isom et al., 2010). Maintenance of the native structure by these forces is highly dependent on the environment (habitat) in which the organism thrives. For example, organisms which are adapted to living under high temperature condition produce proteins which are thermophilic. Although these proteins exhibit an unusual thermostability, their folded native conformations are very much similar to their mesophilic counterparts (Arnold et al., 2001; Motono et al., 2001; Shiraki et al., 2004; Luke et al., 2007). A variety of strategies such as site-directed mutagenesis, chemical modification etc have been employed to elucidate the mechanism of thermostability of these proteins (Declerck et al., 1990; Declerck et al., 1995; Khajeh et al., 2001a). However, studies involving the mechanism of inactivation of thermophilic proteins are not confined to proteins from extremophiles but also involve mesophiles. In this respect, the amylolytic α-amylase is a good example representing thermophilic protein from both thermophiles and mesophiles (Declerck et al., 2002; Fitter, 2005). Besides being a

model protein for thermostability studies, its relevance to biotechnological applications has attracted many researchers (Vieille & Zeikus, 2001).

α-Amylase (α-1,4-glucan-4-glucanohydrolases, EC 3.2.1.1), a member of the family of endoamylases, catalyzes the hydrolysis of α-$_D$-(1,4) glycosidic bonds in starch yielding maltodextrins and glucose (Machius et al., 1995; Nazmi et al., 2006). The enzyme isolated from various sources (bacteria, fungi and yeast) exhibits a broad range of melting temperatures (T_m, 40–110°C) (Darnis et al., 1999; Teotia & Gupta, 2001; Jensen et al., 2003; Wanderley et al., 2004; Hmidet et al., 2008; Kiran & Chandra, 2008; Tripathi et al., 2008). Of these, α-amylases from *Bacillus* species are of special interest for large-scale biotechnological applications due to their thermostability and availability of efficient expression systems (Fitter, 2005). Their biotechnological applications encompass maltodextrin and alcohol production, brewing, baking, textile and detergent industries (Pandey et al., 2000; Ammar et al., 2002; Varavinita et al., 2002; Bessler et al., 2003; Nagarajan et al., 2006). Being highly thermostable (T_m ~ 103°C) (Fitter & Haber-Pohlmeier, 2004), *Bacillus licheniformis* α-amylase (BLA) has been preferred over other α-amylases in starch processing industry employing a high temperature of ~100°C (Janeček & Baláž, 1992). Hence, this monomeric multi-domain protein has been used as a model to understand the mechanism of thermal adaptation (Vihinen & Mäntsälä, 1989; Fitter & Haber-Pohlmeier, 2004; Duy & Fitter, 2005; Fitter, 2005).

2.2. Isolation and purification

α-Amylases are widely distributed in nature and can be obtained from fungi, yeasts as well as bacteria growing on rotting starchy material, soil and air. Among the microorganisms, *Aspergillus sp.*, *Streptomyces sp.* and *Bacillus sp.* are the common sources for α-amylases (Table 2.1). Similar to other enzymes, production of α-amylase

Table 2.1: α-Amylase producing microorganisms.*

Microorganism	**Source**	**Reference**
Fungi		
Aspergillus awamori KT-11	Air	Matsubara *et al.* (2004)
Aspergillus ficum	–	Hayashida & Teramoto (1986)
Aspergillus niger AM07	Soil	Omemu *et al.* (2005)
Penicillium brunneum No. 24	–	Haska & Ohta (1994)
Synnematous sp.	–	Marlida *et al.* (2007)
Streptomyces precox NA-273	–	Takaya *et al.*(1979)
Streptomyces sp No. 4	Soil	Primarini & Ohta (2000)
Thermomyces lanuginosus F1	Municipal compost	Odibo & Ulbrich-Hofmann (2001)
Yeast		
Cryptococcus sp. S-2	–	Lefuji *et al.* (1996)
Bacteria		
Anoxybacillus contaminans	–	Anders *et al.* (2006)
Bacillus amyloliquefaciens	Soil	Demirkan *et al.* (2005)
Bacillus licheniformis	–	Arasaratnam & Balasubramaniam (1992)
Bacillus sp. B1018	–	Itkor *et al.* (1989)
Bacillus sp. I-3	–	Nidhi *et al.* (2005)
Bacillus sp. IMD 434	–	Hamilton *et al.* (1999a)
Bacillus sp. IMD 435	Mushroom compost	Hamilton *et al.* (1999b)

'Table 2.1, continued'

Bacillus sp. TS-23	–	Lin *et al.* (1998)
Bacillus sp. WN11	Hot spring	Mamo & Gessesse (1999)
Bacillus sp. YX-1	Soil	Liu & Xu (2008)
Bacillus stearothermophilus	–	Kim *et al.* (1989)
Bacillus subtilis 65	–	Hayashida *et al.* (1988)
Bacillus subtilis IFO 3108	–	Mitsuiki *et al.* (2005)
Clostridium butyricum T-7	Mesophilic methane sludge	Tanaka *et al.* (1987)
Cytophaga sp.	Soil	Jeang *et al.* (2002)
Geobacillus thermodenitrificans HRO10	–	Ezeji & Bahl (2007)
Streptococcus bovis 148	–	Satoh *et al.* (1997)

*With kind permission from Springer Science + Business Media: <Applied Biochemistry & Biotechnology, Recent advances in microbial raw starch degrading enzymes, 160, 2010, 988–1003, Sun, H., Zhao, P., Ge, X., Xia, Y., Hao, Z., Liu, J., & Peng, M., Table 1).

is also influence by strain, medium composition and culture conditions. Studies have been worked out to enhance the productivity of α-amylases based on screening of potent producers, optimization of medium compositions and culture conditions (Okolo et al., 2000; Hamilton et al., 1999a; Hamilton et al., 1999b; Lin et al., 1998). Different modes of fermentation such as solid-state fermentation (SSF), submerged fermentation (SmF), batch and fed-batch fermentation have been employed to produce α-amylases and the production yield has been found to be affected by each method (Sun et al., 2010). For example, liquid culture of *Rhizopus* strains yielded a higher productivity (4.4 times) than that of solid-state (Morita et al., 1998). Nonetheless, SSF is still preferred due to its simplicity and similarity to the natural growth conditions of organisms (Sun et al., 2010). In bacteria, α-amylases are commonly isolated from *Bacillus* species due to its relatively good recovery rate (~25%) (Najafi & Deobagkar, 2005).

Several purification strategies have been employed to purify α-amylases from various sources and are summarized in Table 2.2. These strategies vary considerably but often involve a series of steps. Purification of extracellular α-amylases from microbial sources usually involves separation of the culture from fermentation broth by centrifugation and/or ultrafiltration, precipitation with ammonium sulfate or organic solvents such as chilled acetone or alcohol. The crude enzyme obtained from these steps is then subjected to various chromatographic techniques such as affinity, ion exchange and/or gel filtration. On the other hand, for the purification of intracellular enzymes, destruction of cell wall is needed prior to the implementation of these procedures mentioned above. Among the different methods used for concentrating enzyme, sucrose solution has been found to be most effective with minimal loss of activity (Okolo et al., 2000). Starch adsorption-elution has also been found as an effective method of enzyme purification due to the adsorption of α-amylases on starch granules

Table 2.2: Purification strategies employed for different α-amylases.*

Microorganism	Purification strategy	Purification fold / yield (%)	Reference
Bacillus licheniformis NH1	40–60% $(NH_4)_2SO_4$ purification→ Sephadex G-100→ Sepharose mono Q anion exchange	3.08 / 15.9	Hmidet et al. (2008)
Bacillus licheniformis	$(NH_4)_2SO_4$ purification→ anion exchange→ gel chromatography	187.1 / 19.5	Liu et al. (2008)
Aspergillus carbonarius	4 M sucrose→ S-Sepharose (fast flow) column→ Q-Sepharose (fast flow) column	2.8 / 12.0	Okolo et al. (2000)
Bacillus sp. IMD 370	Ethanol precipitation→ I DEAE BioGel A chromatography→ II DEAE BioGel A chromatography→ Superose 12 gel filtration	104.3 / 14.9	Mctigue et al. (1995)
Bacillus sp. IMD 434	Acetone precipitation→ ion-exchange (Resource Q column) → hydrophobic interaction chromatography (phenyl-sepharose)	266 / 10	Hamilton et al. (1999a)
	α-Cyclodextrin Sepharose 6B affinity chromatography	375 / 65	Hamilton et al. (1998)
Bacillus sp. IMD 435	α-Cyclodextrin Sepharose 6B affinity chromatography	774 / 65	Hamilton et al. (1999b)
Bacillus sp. TS-23	Raw starch adsorption-elution→ Sephacryl S-100 HR→ HiTrap	708.5 / 13.2	Lin et al. (1998)
Bacillus sp. YX-1	60% $(NH_4)_2SO_4$ fractionation→ DEAE-Sepharose→ Sephadex G-75	34 / 6.6	Liu & Xu (2008)
Cryptococcus sp. S-2	Ultrafiltration→ α-cyclodextrin-Sepharose 6B	141 / 78	Lefuji et al. (1996)
Penicillium sp. X-1	65% $(NH_4)_2SO_4$ fractionation	4.3 / 91	Sun et al. (2007)

‘Table 2.2, continued’

Streptomyces sp. E-2248	Starch adsorption→ DEAE-Toyopearl→ Toyopearl-HW55S	2130 / 60.1	Kaneko et al. (2005)

*With kind permission from Springer Science + Business Media: <Applied Biochemistry & Biotechnology, Recent advances in microbial raw starch degrading enzymes, 160, 2010, 988–1003, Sun, H., Zhao, P., Ge, X., Xia, Y., Hao, Z., Liu, J., & Peng, M., Table 3).

(Kaneko et al., 2005). Both starch adsorptions along with other chromatographic techniques as well as α-cyclodextrin-Sepharose 6B affinity chromatography have been reported to purify α-amylases with high purification fold/yield (Hamilton et al., 1999a).

2.3 Physicochemical properties

Physicochemical properties of BLA are summarized in Table 2.3. Different values of molecular weight of BLA were obtained when determined by sedimentation equilibrium (48,700) and SDS-PAGE (58,000 Da) (Chiang et al., 1979; Damodara Rao et al., 2002). However, Sephadex G-100 gel chromatography yielded a very low value of molecular weight (22,500 Da) (Saito, 1973). Such discrepancy in gel chromatographic data can be attributed to the possible interaction of BLA with Sephadex gel matrix (Kruger & Lineback, 1987). A value of 3.20 nm has been determined for the Stokes radius of BLA using dynamic light scattering method (Fitter & Haber-Pohlmeier, 2004). Ultracentrifugation study has shown the sedimentation coefficient, $S^{o}_{20,w}$ value of BLA as 3.6 s (Saito, 1973). The unit cell dimensions of BLA have been determined as 91.3 × 137.7 Å (Machius et al., 1998). Different values of the isoelectric point for BLA have been reported by different workers using different techniques. While Esteve-Romero et al. (1996) and Chiang et al. (1979) have reported a value of isoelectric point as 7.18 and 5.20 respectively using isoelectric focusing, a value of 6.0 has been obtained by Shaw et al. (2008) using charge ladder technique. Although present in a mesophilic bacterium, BLA has shown unusual hyperthermostability with a melting temperature of 103°C (Fitter & Haber-Pohlmeier, 2004). The emission maximum of BLA has been found at 334 nm when excited at 280 nm due to high content of tryptophan residues (Fitter & Haber-Pohlmeier, 2004). The molar extinction coefficient, ϵ_m at 280 nm of BLA has been determined as 139,690 $M^{-1}.cm^{-1}$ (Nazmi et al., 2006). DSSP database has shown the presence of 26% helical structure (including 21.4% α-helix and 4.6% 3_{10}-helix) and

Table 2.3: Physicochemical properties of BLA.

Property	**Value**	**Reference**
Molecular mass (Da)		
– From sedimentation equilibrium	48,700	Chiang et al. (1979)
– From SDS-PAGE	58,000	Damodara Rao et al. (2002)
– From gel filtration	22,500	Saito (1973)
Stokes radius (nm)		
– Dynamic light scattering	3.2	Fitter & Haber-Pohlmeier (2004)
Isoelectric point		
– Isoelectric focusing	7.18	Esteve-Romero et al. (1996)
– Isoelectric focusing	5.20	Chiang et al. (1979)
– Charge ladder	6.00	Shaw et al. (2008)
Melting temperature, T_m (°C)	103	Fitter & Haber-Pohlmeier (2004)
Sedimentation coefficient, $S^o_{20,w}$, (s)	3.6	Saito (1973)
Unit cell dimensions (Å)	91.3 × 137.7	Machius et al. (1998)
Emission maximum (nm) (upon excitation at 280 nm)	334	Fitter & Haber-Pohlmeier (2004)
ϵ_m at 280 nm ($M^{-1}.cm^{-1}$)	139,690	Nazmi et al. (2006)
Secondary structures		
– Helices (α- and 3_{10}) (%)	26	PDB entry code 1BLI
– β-forms (%)	24	PDB entry code 1BLI

24% β-structures in the native protein (PDB entry code 1BLI).

2.4 Structural organization

2.4.1 Amino acid composition: Table 2.4 shows the amino acid composition of BLA (PDB entry code 1BLI). The protein consists of 483 amino acid residues out of which 41% are hydrophobic in nature. The total number of basic amino acid residues (73) is slightly higher than the total number of acidic amino acid residues (61). The protein is characterized by the abundance of 17 tryptophan and 31 tyrosine residues and lacks the presence of any cycteine residue (PDB entry code 1BLI). BLA has been classified as a simple protein devoid of any carbohydrate moiety. However, the protein has been found to possess one sodium and three calcium ions bound to it (Machius et al., 1998).

2.4.2 Primary structure: BLA is a single polypeptide chain of 483 amino acid residues distributed into three domains namely A, B and C and without any disulfide linkages (Machius et al., 1995). Figure 2.1 shows the primary structure of BLA. The N-terminal domain A comprises of residues 1–101 and 203–396 in the primary sequence of BLA. This is the most conserved domain in α-amylases (Machius et al., 1995). Residues 111–121 and 133–140 make up domain B in BLA which is the least similar region of α-amylases with higher degree of structural complexity (Machius et al., 1998). Domain C (residues 393–483) is generally well-conserved among different α-amylases with the exception of barley α-amylase (Kadziola et al., 1994).

2.4.3 Three-dimensional structure: Three-dimensional structures of different α-amylases have been worked out and are shown in Figure 2.2. Similarities in the three-dimensional structures were noticed among α-amylases, several related amylolytic

Table 2.4: Amino acid composition of *Bacillus licheniformis* α-amylase.*

Amino acid	**No. of residues**
Alanine	35
Arginine	21 (22)
Asparagine	23 (25)
Aspartic acid	37
Glutamic acid	24 (25)
Glutamine	19 (20)
Glycine	46 (45)
Histidine	24
Isoleucine	20
Leucine	29 (28)
Lysine	28
Methionine	7
Phenylalanine	21 (20)
Proline	15
Serine	27 (26)
Threonine	27
Tryptophan	17
Tyrosine	31 (30)
Valine	32
Total	**483**

*PDB entry code 1BLI.

The number of residues in brackets show the variations of the residues obtained from cDNA (Yuuki et al., 1985).

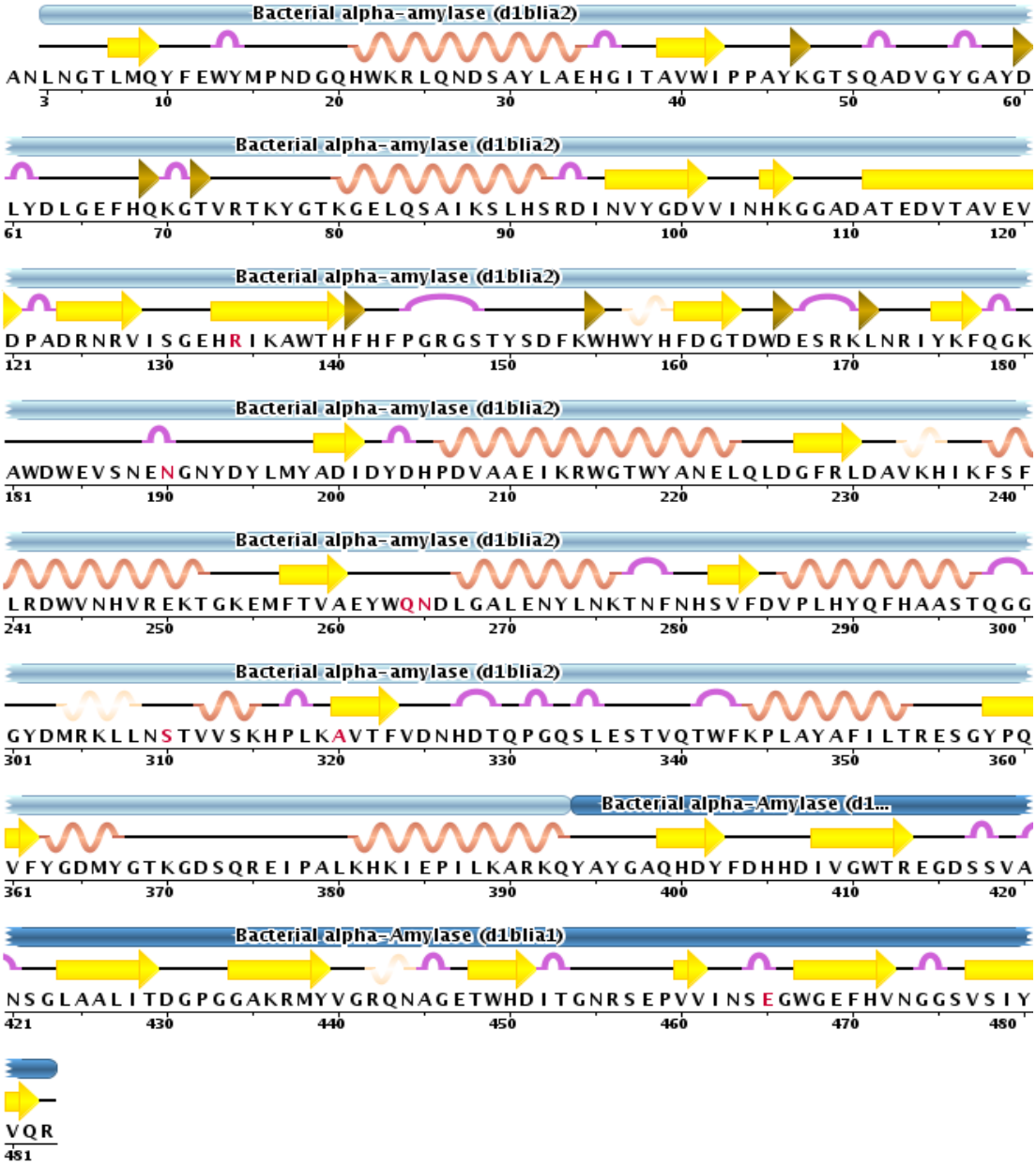

Figure 2.1: Primary structure of BLA. The complete amino acid sequence corresponding to mature BLA is adapted from Protein Data Bank (entry code 1BLI). The position of α-helices and β-sheets as determined from BLA crystal structure (Machius *et al.*, 1998) are indicated by spirals and arrows respectively, coloured in orange and yellow. d1blia1 (dark blue) and d1blia2 (sky blue) refer to glycosyl hydrolase domain and TIM β/α barrel respectively.

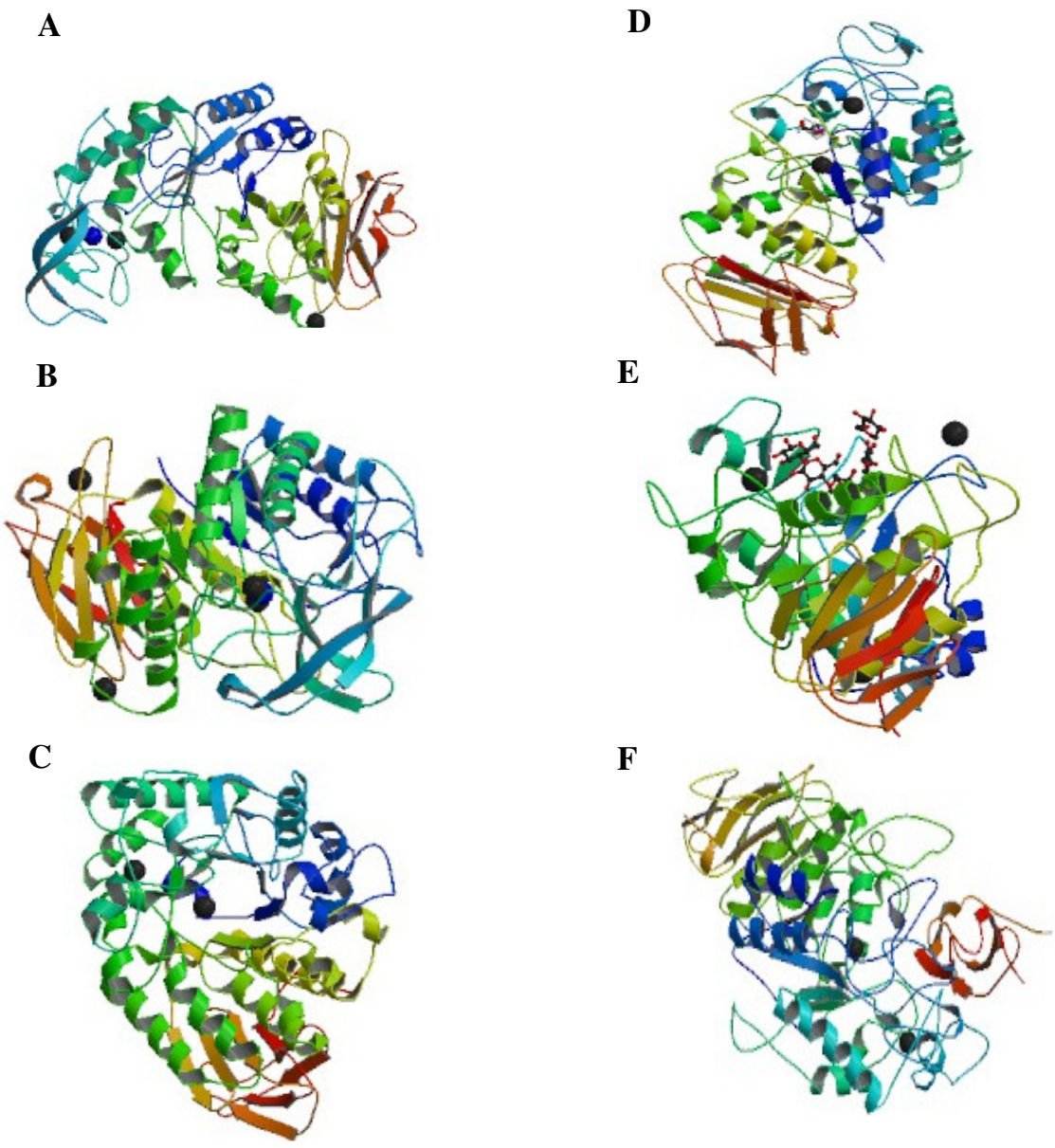

Figure 2.2: Three-dimensional structures of various α-amylases. (A) α-amylase from *Bacillus licheniformis* (PDB entry code 1BLI), (B) α-amylase from *Bacillus amyloliquefaciens* (PDB entry code 3BH4), (C) α-amylase from *Aspergillus oryzae* (TAKA) (PDB entry code 6TAA), (D) α-amylase from *Alteromonas haloplanctis* complexed with Tris (PDB entry code 1AQM), (E) α-amylase from *Bacillus subtilis* complexed with maltopentaose (PDB entry code 1BAG), (F) α-amylase from porcine pancreas (PPA) complexed with the proteinaceous inhibitor Tendamistat (PDB entry code 1BVN).

enzymes *e.g.* cyclodextrin glycosyltransferases (CGT) and α-glycosidases from different organisms despite differences in their amino acid sequences (Machius et al., 1995). Most of them consist of a monomer with 3 domains (domains A, B and C) displaying a β/α-barrel as a central part (domain A). Domain B along with the central domain A constitutes the substrate binding cleft while domain C is positioned opposite to the central β/α-barrel. In addition, at least one calcium binding site is conserved in most α-amylases, which is required to maintain structural integrity of the enzyme (Violet & Meunier, 1989; Feller et al., 1999; Fukada et al., 1987; Fitter et al., 2001; Nielsen et al., 2003; Tanaka & Hoshino, 2002; Vallee et al., 1959; Vihinen & Mäntsälä, 1989). Amino acids involved in substrate binding, chloride binding, calcium binding and catalysis have shown a high degree of homology in different α-amylases (MacGregor & Svensson, 1989; Matsuura et al., 1984; Klein & Schulz, 1991; Jespersen et al., 1991; Kizaki et al., 1993; Qian et al., 1993).

DSSP database (Kabsch & Sander, 1983) revealed the presence of 26% helical structure and 24% β-sheet in BLA (PDB entry code 1BLI). Distribution of different secondary structures in different domains of BLA is given in Table 2.5. All α-helical segments have been found located in domain A while domains B and C are populated with β-strands (Machius et al., 1995). Domain A is characterized by high degree of topological similarity in all known structures of α-amylases. The N-terminal domain A folds into a TIM $(\beta/\alpha)_8$ barrel comprised of 8 segments of α-helices and β-strands each connected by loops involving residues 1–101 and 203–396 in BLA (Figure 2.1) (Machius et al., 1995). The active site, conserved calcium binding site and chloride binding site are housed near the C- terminal side of the barrel (Machius et al., 1998). Remarkable similarities in terms of length, sequence and topological location of each segment were found in domain A of BLA and three other α-amylases (PPA; TAKA and CGT).

Table 2.5: Secondary structure elements of *Bacillus licheniformis* α-amylase as assigned with DSSP (Kabsch & Sander, 1983).*

Domain A		**Domain B**	
Aβ1	Leu7–Gln9	Bβ1	His105–Lys106
Aα1	His21–Glu34	Bβ2	Ala111–Glu119
Aβ2	Ala39–Trp41	Bβ3	His133–His140
Aα2	Lys80–Ser92	$B3_{10}1$	Trp157–His159
Aβ3	Asn96–Val101	Bβ4	Phe160–Asp166
Aα3	Pro206–Leu223	Bβ5	Leu171–Phe177
Aβ4	Gly227–Leu230	$B3_{10}2$	Asp194–Met197
$A3_{10}1$	Val233–His235	Bβ6	Ala199–Ile201
Aα4	Phe238–Thr252		
Aβ5	Phe257–Ala260	**Domain C**	
Aα5	Leu267–Lys276	Cβ1	Gln399–Tyr402
Aβ6	Ser282–Phe284	Cβ2	Ile408–Arg413
Aα6	Val286–Ser296	Cβ3	Leu424–Thr429
$A3_{10}2$	Met304–Leu308	Cβ4	Gly434–Tyr439
α	Val312–Lys315	$C3_{10}$	Arg442–Asn444
$A3_{10}3$	Pro317–Lys319	Cβ5	Thr448–Asp451
Aβ7	Ala320–Phe323	Cβ6	Val460–Val461
$A3_{10}4$	Thr341–Phe343	Cβ7	Trp467–Val472
Aα7	Lys344–Thr353	Cβ8	Val477–Val481
Aβ8	Tyr358–Phe362		
Aα7	Tyr363–Tyr367		
Aα8	Lys381–Gln393		

*Reprinted from Journal of Molecular Biology, 246, Machius, M., Wiegand, G., & Huber, R., Crystal structure of calcium-depleted *Bacillus licheniformis* α-amylase at 2.2 Å resolution, 545–559 (1995), with permission from Elsevier.

β-strands, Aβ1 and Aβ2 have middle range lengths of 3–5 residues whereas Aβ3 has identical length of 6 residues. Both Aβ4 and Aβ5 segments were found to have identical length of 4 residues each. The shortest strands are Aβ6 and Aβ7 with 2–4 residues while Aβ8 is 5 residues long in all three enzymes except for PPA where it is the longest strand with 8 residues. A slight variation was observed in barrel helices. The longest helical segment is Aα3 with 16–18 residues while Aα5 is the shortest with 9–10 residues. In PPA, Aα5 is replaced by a four-residue 3_{10}-helix. Helical segment Aα6 is made up of 11 residues. In BLA, Aα7 is split into 2 parts due to the presence of proline one of which is 3_{10}-helix whereas the presence of proline in Aα8 did not disturb the structure of BLA. In all four α-amylases described above, the barrel symmetry is perturbed by the presence of additional structures between the helices and strands to different extent. In addition to the above similarities observed among different helical and β segments of the four α-amylases, two 3_{10}-helices (β-turns III) located between Aβ4 and Aα4, and before Aα7 were also found similar in all these proteins. Furthermore, connecting loops in all the four enzymes also show similar topology being highest in TAKA and CGT (Machius et al., 1995).

Six loosely connected and twisted antiparallel β sheets constitute domain B in BLA which extends as a protrusion from domain A and shows the least homology in different α-amylases (Machius et al., 1995). Two larger two-stranded sheets (comprised of Bβ3 and Bβ4 as well as Bβ5 and Bβ6) wind around each other in a double-helical fashion and form a barrel with a large interior hole. Spaces between Bβ6 and Bβ3 as well as between Bβ4 and Bβ2 are occupied by the two 3_{10}-helices found as extrusions in domain B. All these characteristics have made domain B to be defined as the folded unit as both terminal ends of this domain also participate in the fold. The possible hydrogen bonding pattern in domain B of BLA is shown in Figure 2.3. β sheets are also common

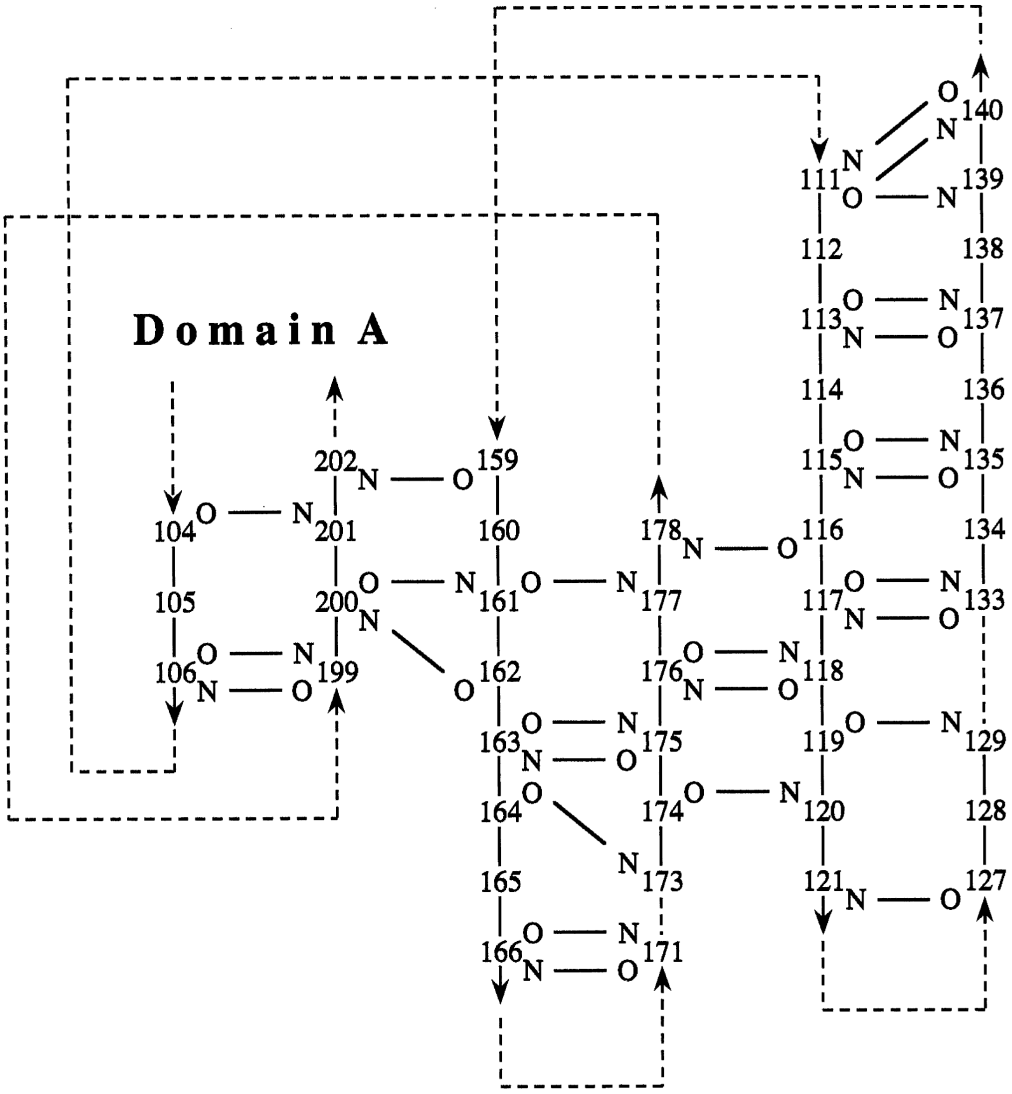

Figure 2.3: A representation of all β structures in domain B of BLA.

Reprinted from Journal of Molecular Biology, 246, Machius, M., Wiegand, G., & Huber, R., Crystal structure of calcium-depleted *Bacillus licheniformis* α-amylase at 2.2 Å resolution, 545–559 (1995), with permission from Elsevier.

in domain B of other α-amylases albeit with lesser complexity. A six-residue helical segment commonly found in these α-amylases is absent in BLA. The C-terminal domain (domain C) in all four α-amylases contains an invariable Greek key motif (Richardson, 1981). All these proteins are similar in the overall topology of domain C except for the presence of a 3_{10}-helix after Cβ4 in BLA (Machius et al., 1995).

2.4.4 Active site, metal binding sites and ionic interactions: Two aspartic acid and one glutamic acid residues located on the C-terminal side of the central β-barrel were proposed earlier as catalytic residues for TAKA and PPA (Matsuura et al., 1984; Buisson et al., 1987; Qian et al., 1993). These three catalytic residues along with a few more residues in the vicinity were found strictly conserved in all four α-amylases (Table 2.6) described above (Klein & Schulz, 1991; Kizaki et al., 1993; Juncosa et al., 1994; Holm et al., 1990; Machius et al., 1995). All these residues are supposed to play an important role in the substrate binding. The structure of PPA complexed with protein inhibitor Tendamistat (Figure 2.2F) (Wiegand et al., 1995) showed a strong hydrophobic interaction together with specific hydrogen bonds between the protein and the ligand which should also be expected for natural substrate binding.

The first calcium binding site (Ca I) was found to reside between domain B and C-terminus of the central $(\beta/\alpha)_8$ barrel and is well conserved (Machius et al., 1998). Second calcium binding site (Ca II) found in the same domain of BLA is also well conserved in α-amylases with more than one calcium binding site (Machius et al., 1998). The two calcium ions bound to these two sites along with a sodium ion form a Ca-Na-Ca metal triad. Most of the contacts between metal triad and the enzyme are made with domains B leaving 2 interactions with domain A residues. A total of 11 residues along with 2 water molecules make 20 interactions with this triad including

Table 2.6: Residues involved in the active site of different α-amylases.*

BLA	**PPA**	**TAKA**	**CGT**	
Asp231	Asp197	Asp206	Asp229	Strictly conserved
Asp328	Asp300	Asp297	Asp328	Strictly conserved
Glu261	Glu233	Glu230	Glu257	Strictly conserved
Gln9	Phe13	His15	Gln19	Not conserved
Tyr56	Tyr82	Tyr62	Tyr100	Strictly conserved
Asp100	Asp117	Asp96	Asp135	Strictly conserved
Val102	Val119	Val98	Ala137	Qualitatively conserved
Lys234	Lys209	Lys200	Lys232	Strictly conserved
Val259	Ile228	Phe231	Phe255	Qualitatively conserved
Trp263	Leu232	Ile235	Phe259	Qualitatively conserved
His327	His296	His299	His237	Strictly conserved

*Reprinted from Journal of Molecular Biology, 246, Machius, M., Wiegand, G., & Huber, R., Crystal structure of calcium-depleted *Bacillus licheniformis* α-amylase at 2.2 Å resolution, 545–559 (1995), with permission from Elsevier.

seven interactions with each calcium ion and six interactions with sodium ion. The surrounding of metal triad is highly negatively charged and dominated by 6 aspartate residues. Thirteen atoms of the aspartate side chains contribute towards 20 interactions. The binding of each metal ion with one of the aspartate is in the bidendate mode and shares 2 aspartate residues with neighbouring metal ion. In addition, 4 carbonyl oxygen atoms, one asparagine OD1 chain and one water molecule flanking each calcium ion also participate. Different amino acid residues along with the binding atoms in BLA and their distances with the metal ions in a metal triad are given in Table 2.7. The architecture of the calcium binding site can be seen as a distorted pentagonal bipyramid in *Aspergillus niger* α-amylase (Boel et al., 1990) and is found to be the same in BLA (Machius et al., 1998). Presence of an unusual *cis* peptide bond between tryptophan 184 and glutamate 185 is the unique characteristic of the site surrounding metal triad and is suggested to be essential for the correct structure of the metal binding site (Machius et al., 1998). This *cis* peptide conformation is believed to be stabilized by the ionic interaction between the glutamate side chain and lysine 276 of BLA.

The interface between domains A and C (Figure 2.4) houses the third calcium binding site (Ca III) which was not observed earlier with other α-amylases (Machius et al., 1998). The calcium ion bound to Ca III site connects two loops in domain C with a large loop in domain A and is positioned on the C-terminal side of the central $(\beta/\alpha)_8$ barrel exactly opposite to the hinge region showing joining of domains A and C in BLA. Three aspartate side chain atoms, 3 carbonyl oxygen atoms and one water molecule coordinate with calcium at Ca III binding site. However, the coordination geometry of Ca III differs from Ca I and Ca II in being the *trans* position to the bidendate aspartate occupied by a water molecule (Machius et al., 1998). Similar degree of conservation was also found for chloride binding site which is located near calcium

Table 2.7: Distances between the metal ions in BLA and their ligands.*

Metal ion	**Ligand**	**Distance (Å)**
Calcium I		
	Asn104 OD1	2.4
	Asp194 O	2.4
	Asp194 OD1	2.5
	Asp200 OD1	2.4
	Asp200 OD2	3.0
	His235 O	2.4
	Wat	2.6
Calcium II		
	Asp161 OD1	2.6
	Asp161 OD2	2.6
	Ala181 O	2.4
	Asp183 OD1	2.4
	Asp202 OD2	2.5
	Asp204 OD1	2.6
	Wat	2.6
Calcium III		
	Gly300 O	2.6
	Tyr302 O	2.3
	His406 O	2.6
	Asp407 OD2	2.3
	Asp430 OD1	2.6
	Asp430 OD2	2.6
	Wat	2.9
Sodium		
	Asp161 OD1	2.4
	Asp183 OD2	2.7
	Asp194 OD1	3.1
	Asp194 OD2	2.5
	Asp200 OD2	2.4
	Ile201 O	2.5

*Reprinted from Structure, 6, Machius, M., Declerck, N., Huber, R., & Wiegand, G., Activation of *Bacillus licheniformis* α-amylase through a disorder → order transition of the substrate-binding site mediated by a calcium-sodium-calcium metal triad, 281–292 (1998), with permission from Elsevier.

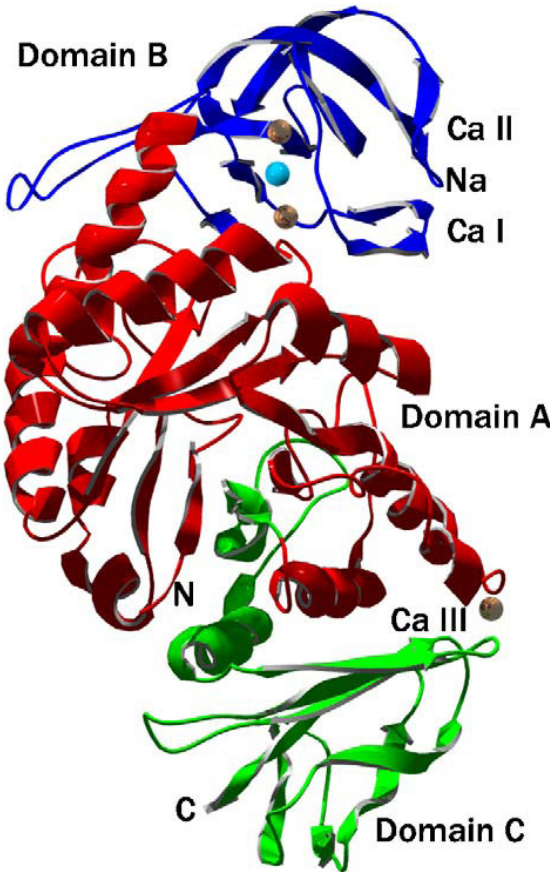

Figure 2.4: Tertiary structure of *Bacillus licheniformis* α-amylase (PDB entry 1BLI). The calcium and sodium ions bound to the protein in its native form are shown. Domain A, shown in red, is a β/α TIM barrel. Domain B is colored in blue and domain C in green. The three calcium ions are shown in gold and the sodium ion is shown in blue.

binding site. The chloride ion is tetra coordinated with NH2 of Arg 229, ND2 of Asn 326 and two water molecules (Machius et al., 1995).

Apart from calcium ion binding which maintains structural stability, several ionic interactions contribute substantially towards maintaining the integrity of the protein (Table 2.8). These interactions function to connect loops to helices, stabilize secondary structural elements viz. helices and the β-barrel strands. Salt bridges between Asp 60 and Arg 146, Asp 204 and Lys 237 connect domains A and B while a salt bridge between Arg 354 and Asp 401 connects domains A and C. A few ionic interactions occurring around the active site are conserved among different α-amylases *i.e.* BLA, CGT, PPA and TAKA.

2.5 Stability

There are several aspects of stability with reference to α-amylases. Tolerance towards a particular environment with certain pH, temperature, surfactants / detergents and chemical denaturants reflects the stability of α-amylases with respect to each condition.

2.5.1 pH: The stable pH range differs among different α-amylases obtained from various sources. For example, α-amylases from *Thermus filiformis* and *Bacillus subtilis* have a wide stable pH range of 4.0–8.0 (Egas et al., 1998) and 4.0–9.0 (Nagarajan et al., 2006) respectively (Table 2.9). The pH-stability profiles of α-amylases from honey and *Bacillus licheniformis* have shown the enzymes' stabilities in the neutral to alkaline pH range, 7.0–8.0 (Babacan & Rand, 2007) and 7.0–9.0 (Krishnan & Chandra, 1983) respectively. BLA has been shown to possess an activity of 95% at pH 10.0, 84% at pH 6.0, 74% at pH 5.0, 68% at pH 4.0 and 50% at pH 3.0 (Krishnan & Chandra, 1983). On the other hand, α-amylase from *Clostridium acetobutylicum* has been found

Table 2.8: Ionic interactions in BLA.*

Atom 1	Atom 2	Distance (Å)	Domains involved
Asp18-OD1	Arg24-NH1	3.1	A–A
Asp18-OD1	Arg24-NH2	3.2	A–A
Asp18-OD2	Arg24-NH2	2.8	A–A
Lys23-NZ	Glu82-OE1	2.8	A–A
Lys47-NZ	Asp63-OD1	2.8	A–A
Lys47-NZ	Asp63-OD2	3.3	A–A
Asp60-OD1	Arg146-NH1	2.7	A–B
Asp60-OD2	Arg146-NH1	2.8	A–B
Glu66-OE2	Lys80-NZ	2.9	A–A
Lys80-NZ	Glu222-OE2	2.9	A–A
His91-NE2	Asp226-OD1	2.9	A–A
Asp100-OD2	Arg229-NH1	3.2	A–A
Glu113-OE1	His156-ND1	2.8	B–B
Asp114-OD2	Lys136-NZ	3.0	B–B
Asp121-OD1	Arg127-NH1	3.1	B–B
Arg125-NH2	Asp164-OD2	3.3	B–B
Asp166-OD1	Arg169-NE	2.8	B–B
Asp166-OD1	Arg169-NH1	3.1	B–B
Glu167-OE1	Lys170-NZ	3.0	B–B
Asp204-OD2	Lys237-NZ	3.0	B–A
Arg229-NH1	Asp231-OD2	3.0	A–A
Arg229-NH2	Glu261-OE2	3.4	A–A
Arg242-NH1	Asp243-OD2	2.6	A–A
Glu250-OE1	Lys251-NZ	3.1	A–A
Glu271-OE1	Lys315-NZ	3.5	A–A
Glu271-OE2	His316-NE2	3.3	A–A
Asp303-OD1	Arg305-NH2	2.9	A–A
Asp303-OD2	Arg305-NE	2.9	A–A
Asp303-OD2	Arg305-NH2	3.5	A–A
Asp325-OD1	Lys344-NZ	2.9	A–A
Glu336-OE1	Arg375-NH2	2.7	A–A
Lys344-NZ	Asp365-OD1	2.8	A–A
Arg354-NH2	Asp401-OD1	2.7	A–C
Arg354-NH2	Asp401-OD2	3.2	A–C
Lys381-NZ	Glu385-OE2	3.1	A–A
His400-NE2	Glu414-OE1	2.7	C–C
Asp404-OD1	Lys436-NZ	2.9	C–C
His406-ND1	Asp407-OD2	3.2	C–C
Arg456-NH1	Glu458-OE1	3.1	C–C

Ionic interactions occurring at a distance <3.5Å between charged atoms are shown.

*Reprinted from Journal of Molecular Biology, 246, Machius, M., Wiegand, G., & Huber, R., Crystal structure of calcium-depleted *Bacillus licheniformis* α-amylase at 2.2 Å resolution, 545–559 (1995), with permission from Elsevier.

Table 2.9: Stable pH ranges of some α-amylases.

Source	**Stable pH range**	**Reference**
Bacillus licheniformis	7.0–9.0	Krishnan & Chandra (1983)
Bacillus subtilis	4.0–9.0	Nagarajan et al. (2006)
Streptococcus bovis	5.5–8.5	Freer (1993)
Thermus filiformis	4.0–8.0	Egas et al. (1998)
Thermococcus profundus	5.9–9.8	Chung et al. (1995)
Penicillium chrysogenum	5.0–6.0	Balkan & Ertan (2005)
Clostridium acetobutylicum	3.0–5.5	Paquet et al. (1991)
Honey	7.0–8.0	Babacan & Rand (2007)

to remain stable under acidic pH range, 3.0–5.5 (Paquet et al., 1991). *Penicillium chrysogenum* α-amylase has shown a narrow range of its stability between pH 5.0 and 6.0 (Balkan & Ertan, 2005). α-Amylases showing stability from acidic to alkaline pH range have also been obtained from *Streptococcus bovis* and *Thermococcus profundus* with stability ranges as pH 5.5–8.5 (Freer, 1993) and pH 5.9–9.8 (Egas et al., 1998) respectively.

Acid denaturation studies of BAA and BLA have been made over a pH range of 7.0 to 2.0 using fluorescence spectroscopy which showed a decrease in fluorescence with a start of transition at pH 7.0 and 6.0 and end points at pH 4.0 and ~2.5 respectively (Shokri et al., 2006). A comparison of alkaline denaturation studies over a pH range, 8.0–13.0 made on TAKA, BLA and phosphoglycerate kinase (PGK) have shown the start of unfolding transition at pH 9.5 for TAKA while BLA and PGK started to unfold at pH 11.0. However, only TAKA and PGK have demonstrated partial reversibility of unfolding whereas BLA denaturation has been found to be irreversible unless protecting osmolytes are present in the incubation medium (Strucksberg et al., 2007).

2.5.2 Temperature: Most α-amylases are known to exhibit temperature optima between 40 and 65°C (Sun et al. 2010). Exceptions to this have been noticed with hyperthermostable α-amylases from *Bacillus sp.* such as BLA (optimum temperature = 90°C) (Fitter et al., 2001). This hyperthermostability of α-amylases has been shown to be affected by substrate, calcium, carbohydrate moiety, etc. The stabilizing effect of calcium ions can be attributed to the salting-out of hydrophobic residues by these ions in the protein interior leading to the adoption of a more compact structure (Sun et al., 2010).

Temperature stability of various α-amylases in terms of melting temperature, T_m as well as half life, $T_{1/2}$ has been studied using calorimetry and spectroscopic techniques. Loss of both secondary and tertiary structures of the enzyme has led to its inactivation at high temperatures. BLA has shown a much longer $T_{1/2}$ (270 min) compared to BAA (2 min) and *Bacillus stearothermophilus* (BStA) (50 min) under similar reaction conditions at 90°C, pH 6.5 (Declerck et al., 2002).

Most α-amylases possess one or more calcium binding sites which contribute substantially to their thermostabilities. Almost all α-amylases are stabilized by calcium at high temperatures. Melting temperature of α-amylases varies in the absence and presence of calcium by 14–50°C (Fitter, 2005). In the case of two homologous enzymes, BAA and BLA, a huge difference of 50°C in T_m has been observed in presence of calcium. Although calcium offers significant increase in their thermostabilities, the specific difference in the thermostability between BAA and BLA remains the same (~15°C) both in the absence and presence of calcium. Hence, this appears to be related to the intrinsic property of the protein structures themselves (Fitter & Haber-Pohlmeier, 2004). *Bacillus subtilis* α-amylase (BSUA), similar to BLA in terms of possessing three calcium binding sites has shown a large difference in melting temperature (37°C) upon calcium binding compared to TAKA (two calcium binding sites) and PPA (one calcium binding site) (Fitter, 2005). These results suggest a positive correlation of calcium binding towards enhancing thermostability of α-amylases.

Different α-amylases such as BAA, BLA, PPA and TAKA have shown cooperative thermal transition when monitored by techniques of tryptophan (Trp) fluorescence, circular dichroism (CD) spectroscopy and differential scanning calorimetry (Fitter & Haber-Pohlmeier, 2004; Fukada et al., 1987). With the exception of α-amylase from

Alteromonas haloplanctis (AHA), most α-amylases exhibit irreversible thermal unfolding transition. In addition to this, AHA has shown a narrower transition width and exhibited a pure two-state transition (~10°C transition at 1°C/min heating rate) as noticed with other α-amylases (Feller et al., 1999).

2.5.3 Surfactants / Detergents: *Geobacillus thermoleovorans*, an archeabacteria living in habitats with extremely high temperature produces α-amylase which is resistant towards some surfactants. The enzyme's stability is enhanced in the presence of Tween 20, 40 and 80 whereas it is destabilized to different extent in the presence of a non-ionic detergent, Triton X-100, glycerol, glycine, dextrin and an anionic detergent, SDS (Uma and Satyanarayana, 2007).

α-Amylase isolated from *Bacillus licheniformis* NH1 on the other hand, has shown remarkable stability towards SDS, Triton X-100 as well as Tween 20 (Hmidet et al., 2008). Moreover, the enzyme has shown utmost compatibility with a broad range of commercial liquids and solid detergents at 40℃ thus making it a suitable enzyme for use in the detergent industry. In addition, BLA NH1 is rather stable towards oxidizing agent, maintaining 57% of its initial activity in the presence of 1% (w/v) sodium perborate upon incubation for 1 hour which enables the enzyme to withstand the bleaching agent added with detergent in clothes washing. Likewise, α-amylase produced by a moderately halophilic *Bacillus sp.* strain TSCVKK has been found surfactant- and detergent-stable (Kiran & Chandra, 2008).

2.5.4 Chemical denaturants: Urea-induced denaturation of BAA has shown a cooperative transition when probed spectrophotometrically and Gibs energy changes have been determined in the range of 8–15 kcal/mol (Shareghi et al., 2007). BStA on the

other hand, has been found resistant against urea even at highest urea concentration of 8.0 M at 37°C (Pfueller & Elliot, 1969). The only urea denaturation study of BLA has been reported by Nazmi et al. (2006) using CD spectroscopy. They have shown that in the presence of intrinsic calcium ions bound to the three calcium binding sites available in BLA, the protein remains stable even in the presence of the highest urea concentration (9.0 M). On the other hand, denaturation experiments with calcium depleted (Ca-depleted) form of the enzyme have shown a cooperative transition starting at 1.0 M urea with an end-point at 4.0 M urea concentration suggesting reduced stability of the enzyme due to loss of intrinsic calcium.

GdnHCl denaturation of BLA has been studied using fluorescence and CD spectroscopy (Fitter & Haber-Pohlmeier, 2004; Duy & Fitter, 2006; Strucksberg et al., 2007). Unfolding of BLA has been shown to start at a low GdnHCl concentration (1.5 M) using shift in emission maximum. Even at 6.0 M GdnHCl, fully unfolded BLA remains soluble without any tendency of aggregation (Strucksberg et al., 2007). GdnHCl denaturation of BAA has shown the presence of a partially folded intermediate state at 1.0 M GdnHCl, suggesting a three-state transition when probed by 8-anilino-1-napthalene sulfonic acid (ANS) (Zheng et al., 2009). Fluorescence quenching studies with potassium iodide has revealed the number of accessible Trp residues in partially folded intermediate as eight and GdnHCl denaturation of BAA has been found free from any aggregation even at the highest (6.0 M) concentration (Zheng et al., 2009). Using intrinsic fluorescence and proteolytic degradation techniques, GdnHCl denaturation of BSUA has been found reversible at pH 7.0 and 37°C (Haddaoui et al., 1997). The first renaturation step has shown the conversion from a totally denatured state to a partially-structured state of the protein in less than 1 second. This intermediate has been found resistant against proteolytic degradation and requires calcium for its

transformation into the native state (Haddaoui et al., 1997). This indicates that presence of intrinsic calcium also enhances stability of the enzyme against GdnHCl denaturation apart from providing thermostability as reported earlier (Fitter & Haber-Pohlmeier, 2004; Fitter 2005; Duy & Fitter, 2006).

Based on the above literature review, it appears that salt bridges play an important role in maintaining the structural stability of BLA. Furthermore, calcium ions are supposed to enhance stability of α-amylases against various denaturants. Hence, lysine residues of BLA were modified using succinic anhydride (to convert the positive charge on lysine residues into negative charge), potassium cyanate (to abolish the positive charge on lysine residues) and O-methylisourea (to maintain the positive charge but with an additional small hydrophobic group) and the effect of charge imbalance on the conformation as well as the conformational stability of BLA was studied. Role of calcium in the stability against urea and GdnHCl denaturations of native and Ca-depleted BLAs were also investigated.

CHAPTER 3

MATERIALS AND METHODS

3.1 Materials

3.1.1 Proteins

α-Amylase from *Bacillus licheniformis* (93–100% by SDS-PAGE) (lot 018K7008) was obtained from Sigma Chemical Company, USA. Various marker proteins such as bovine serum albumin (lot 015K0591), carbonic anhydrase (lot 99H0669), α-chymotrypsinogen A (lot 16H7075) and cytochrome c (lot 27H7065) were also supplied by Sigma Chemical Company, USA.

3.1.2 Reagents used in protein estimation

Sodium carbonate, potassium sodium tartarate, copper sulfate and hydrochloric acid were purchased from SYSTERM®, Malaysia. Folin-Ciocalteu reagent was procured from Merck, Germany. It was diluted with water in a ratio of 1:3 before use.

3.1.3 Reagents used in enzyme assay

Maltose (lot PHRM160306) was obtained from R & M Chemicals, UK while 3, 5-dinitrosalicylic acid (lot 037K3721) was the product of Sigma Chemical Company, USA. Starch from potatoes (lot 13311230) was purchased from Fluka, Germany.

3.1.4 Reagents used in chemical modification

Succinic anhydride (lot 1317409), potassium cyanate (lot 1330892) and O-methylisourea hydrogen sulfate (lot 1284478) were the products of Fluka, Germany. 2, 4, 6-Trinitrobenzenesulfonic acid (lot 28999) was procured from Pierce Chemical

Company, USA. Dimethyl sulfoxide (DMSO) was supplied by Merck, Germany while sodium dodecyl sulfate (SDS) was obtained from SYSTERM®, Malaysia.

3.1.5 Reagents used in polyacrylamide gel electrophoresis

N, N'-Methylenebisacrylamide (lot 20H0403), N, N, N', N'-tetramethylethylenediamine (TEMED) (lot 41K1263) and ammonium persulfate (lot 39H1089) were purchased from Sigma Chemical Company, USA. Acrylamide (lot 9270291) and bromophenol blue (lot 6257909) were obtained from Merck, Germany. Tris (hydroxymethyl)-aminomethane (lot 0906B070) and coomassie brilliant blue R-250 (lot 1610435) were the products of AMRESCO, USA and Bio-Rad Laboratories, USA respectively. Glycerol, glycine, acetic acid and methanol were obtained from SYSTERM®, Malaysia.

3.1.6 Reagents used in gel chromatography

Sephacryl S-200 HR (lot 116K0771) and blue dextran (lot 066K1083) were purchased from Sigma Chemical Company, USA. L-Tyrosine (lot 6380446) was procured from Merck, Germany.

3.1.7 Reagents used in denaturation experiments

Urea SigmaUltra (lot 027K00591) and guanidine hydrochloride (≥ 99 %) (lot 027K5419) were supplied by Sigma Chemical Company, USA.

3.1.8 Miscellaneous

Ethylene glycol-bis (2-aminoethyl-ether)-N,N,N',N'-tetraacetic acid (EGTA), standard buffers of pH 7.0; 4.0 and dialysis tubing of 27 mm diameter were procured from Sigma Chemical Company, USA. Analytical grade reagents of sodium dihydrogen phosphate,

disodium hydrogen phosphate, sodium hydroxide (NaOH), sodium chloride (NaCl), sodium hydrogen carbonate, sodium acetate and calcium chloride-dihydrate ($CaCl_2$) were purchased from SYSTERM®, Malaysia. Filter circles (90 and 125 mm) were obtained from Whatman®, Schleicher & Schuell, England. Parafilm 'M' was the product of Pechiney Plastic Packaging, USA. PVDF membrane Millex HV syringe driven filter units were obtained from Millipore Corporation, Ireland.

All glass distilled water was used throughout these studies and experiments were performed at room temperature (~ 25°C) unless otherwise stated.

3.2 Methods

3.2.1 pH measurements

pH measurements were made on Mettler Toledo pH meter, Delta 320, China using a BNC's combined electrode, type HA405-K2/120 consisting of glass and reference electrodes in a single entity. Standard buffers of pH 4.0 ± 0.01 and pH 7.0 ± 0.01 were used to calibrate the pH meter in the acidic range and neutral to alkaline range respectively.

3.2.2 Absorption spectroscopy

Absorption measurements were made on a Shimadzu double beam Spectrophotometer, model UV-2450, Japan. Quartz cuvettes of 1 cm path length were used for absorption measurements in the ultraviolet (UV) range while glass cuvettes of 1 cm path length were employed in the visible range. Scattering corrections, if required, were made by extrapolation of absorbance values in the wavelength range, 360–340 nm to the desired wavelength.

3.2.3 Fluorescence spectroscopy

Fluorescence measurements were carried out on a Hitachi Fluorescence Spectrophotometer, model FL-2500, Japan equipped with a data recorder. The fluorescence spectra were recorded at a protein concentration of 0.1 μM with a 1 cm path length quartz cuvette. Both excitation and emission slits were set at 10 nm each. Intrinsic fluorescence was read in the wavelength range, 300–400 nm after exciting the protein solution at 280 nm. Values of fluorescence intensity were transformed into relative fluorescence intensity by taking the fluorescence intensity of *Bacillus licheniformis* α-amylase (BLA) at its emission maximum in the absence of guanidine hydrochloride (GdnHCl) as 100. The data were plotted as relative fluorescence intensity versus GdnHCl concentration.

3.2.4 Circular dichroism spectroscopy

Circular dichroism (CD) measurements were made in the far-UV region (200–250 nm) on a Jasco Spectrometer, model J-810, Japan equipped with a thermostatically controlled cell holder under constant nitrogen flow. The instrument was calibrated with (+)-10-camphorsulfonic acid and the response time was 1 second with a scan speed of 100 nm/min. CD measurements were recorded using a 2 mm path length cell, averaged over three scans and corrected with suitable blanks. The protein concentration used was 0.1 mg/ml (1.8 μM). Results are expressed as mean residue ellipticity (MRE) in deg. cm^2. $dmol^{-1}$ using the relation: $MRE = \theta_{obs} \times (MRW / 10 \times l \times c)$, where θ_{obs} is the measured ellipticity at 222 nm in millidegrees; l is the optical path length of the cell in cm; c is the protein concentration in mg/ml and MRW is the mean residue weight (molecular weight of the protein divided by the total number of amino acid residues). MRE data were transformed into relative MRE by taking the MRE value of the protein in the absence of denaturant as 100.

3.2.5 Preparation of calcium-depleted BLA

Calcium-depleted BLA (Ca-depleted BLA) was prepared following the method of Nazmi et al. (2006) with slight modification. Native BLA (commercial preparation) was dissolved and dialyzed against 40 mM Tris / 20 mM EGTA buffer, pH 7.2 overnight with a minimum of three changes with the same buffer (Nazmi et al., 2006). This step was followed by the removal of EGTA from the sample by dialysis against 20 mM Tris-HCl buffer, pH 7.5. All steps were carried out at 4°C and plastic vessels were used instead of glass to avoid calcium ions contamination.

3.2.6 Determination of protein concentration

Protein concentration was determined both spectrophotometrically and by the method of Lowry et al. (1951) using bovine serum albumin as the standard.

3.2.6.1 Spectrophotometric method

Protein concentrations of both native and Ca-depleted BLA were determined spectrophotometrically using a molar extinction coefficient of 139,690 $M^{-1}.cm^{-1}$ at 280 nm (Nazmi et al., 2006).

3.2.6.2 Method of Lowry et al. (1951)

The method involved the use of alkaline copper reagent and Folin-Ciocalteu reagent. Alkaline copper reagent was prepared fresh by mixing 1 volume of 4% (w/v) potassium sodium tartarate to 100 volumes of 4% (w/v) sodium carbonate and finally adding 1 volume of 2% (w/v) copper sulfate to the mixture.

Two standard curves were prepared in two different buffer systems *i.e.* 0.06 M sodium phosphate buffer, pH 7.0 and 0.02 M Tris-HCl buffer, pH 7.5. Increasing volumes of stock protein solution (5 mg/10 ml for phosphate buffer; 10 mg/10 ml for Tris buffer) in the range of 0.1–1.0 ml were taken in different tubes and the final volume in each tube was made up to 1.0 ml, if necessary, with respective buffers. Subsequently, 4.0 ml of freshly prepared alkaline copper reagent was added to all tubes and the contents were vortexed for homogeneous mixing. Upon 10 minutes incubation at room temperature, 1.0 ml of diluted Folin-Ciocalteu reagent was added immediately to all tubes and mixed well. The tubes were further incubated for 30 minutes at room temperature and the color intensity was read at 700 nm against a suitable blank, which was prepared in the same way as for all other tubes except that buffer was used in place of protein solution. The standard curves were plotted between absorbance at 700 nm and amount of protein (Figure 3.1) which yielded the following two straight line equations in respective buffer systems:

$$(\text{Absorbance})_{700\ \text{nm}} = 1.81\ (\text{Amount of protein, mg}) + 0.04 \qquad \text{(Phosphate buffer)} \quad (1)$$

$$(\text{Absorbance})_{700\ \text{nm}} = 0.75\ (\text{Amount of protein, mg}) + 0.01 \qquad \text{(Tris buffer)} \quad (2)$$

3.2.7 Analytical methods

Concentrations of stock urea and GdnHCl solutions were determined from the data of Warren & Gordon (1966) and Nozaki (1972) respectively as described by Pace et al. (1989).

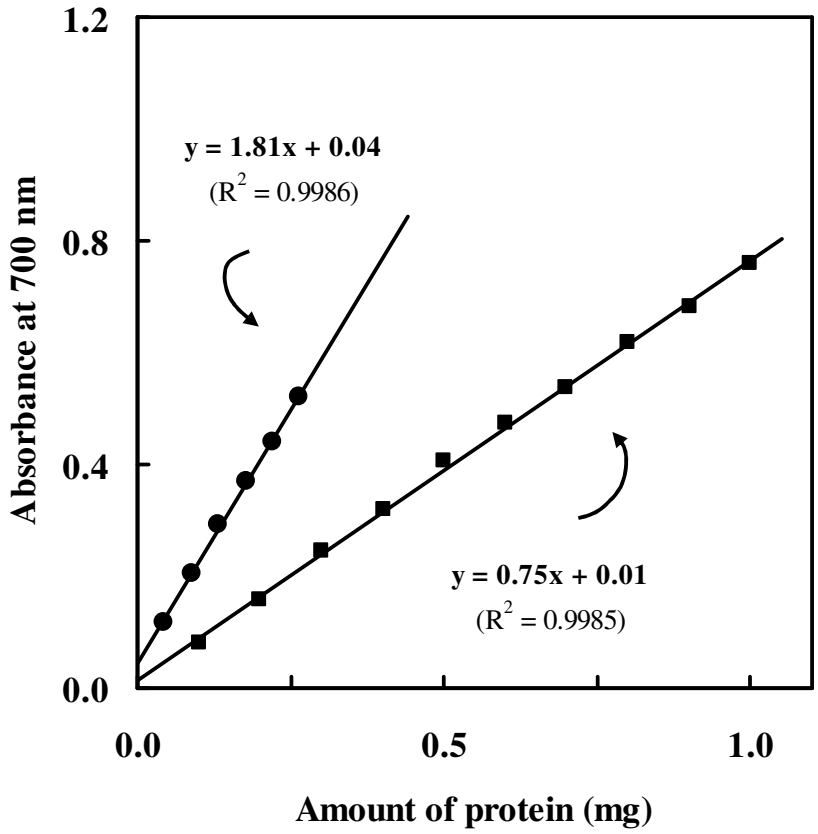

Figure 3.1: Standard curves for the determination of protein concentration by the method of Lowry et al. (1951) using bovine serum albumin as the standard. Standard curves were made in two different buffer systems: 0.06 M sodium phosphate buffer, pH 7.0 (●) and 0.02 M Tris-HCl buffer, pH 7.5 (■). Straight lines were drawn by the method of least squares.

3.2.8 Enzyme assay

The activity of α-amylase was determined according to the method of Bernfeld (1951) using maltose as the standard. This method involved the use of dinitrosalicylic acid (DNS) reagent which was prepared fresh for each assay. DNS reagent was prepared by dissolving 1.0 g of 3, 5-dinitrosalicylic acid in 50 ml of water, followed by the addition of 30 g of potassium sodium tartarate and 20 ml of 2 N NaOH. The final volume was made up to 100 ml with water.

For the preparation of maltose standard curve, increasing volumes of stock maltose solution (18 mg/10 ml of reaction buffer *i.e.,* 0.02 M sodium phosphate buffer, pH 6.9 containing 6 mM NaCl) in the range of 0.1–1.0 ml were taken in different tubes and the final volume in each tube was made up to 1.0 ml, if necessary, with the same buffer. Then 1.0 ml of DNS reagent was added to all tubes and the contents were mixed well. Tubes were incubated in boiling water bath for 5 minutes and cooled down to room temperature under running tap water. Ten milliliters of water was added into each tube, vortexed and absorbance was measured at 540 nm against appropriate blank, prepared in the same way but without maltose solution. A standard curve was plotted between absorbance at 540 nm against amount of maltose (Figure 3.2) which yielded the following straight line equation:

$$(\text{Absorbance})_{540\ \text{nm}} = 0.48\ (\text{Amount of maltose, mg}) - 0.02 \qquad (3)$$

The substrate solution was prepared by dissolving 1.0 g of starch in 100 ml of the reaction buffer. For activity measurements of native and Ca-depleted BLAs, 0.5 ml of diluted enzyme solution containing 4.4 μg of enzyme in reaction buffer was added to 0.5 ml of starch solution and incubated for 3 minutes at room temperature. This was

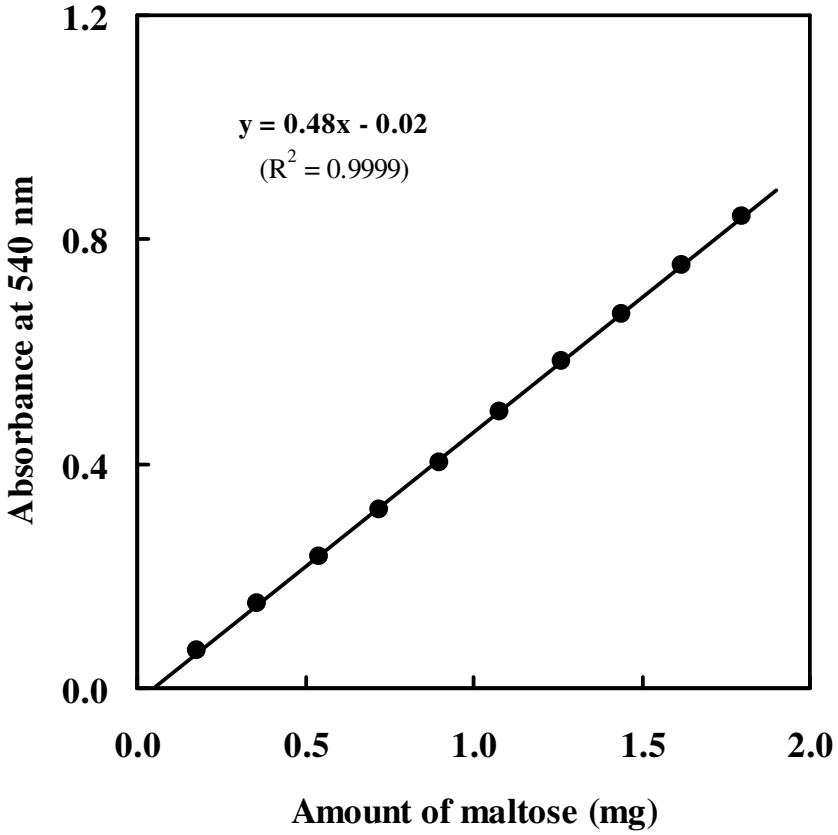

Figure 3.2: Standard curve for the determination of maltose concentration, produced in the activity assay of BLA by the method of Bernfeld (1951). Straight line was drawn by the method of least squares.

followed by the addition of 1.0 ml of DNS reagent. Rest of the procedure was similar as described for the preparation of maltose standard curve. One unit of enzyme was defined as the amount of enzyme required to liberate 1.0 mg of maltose from starch per minute at pH 6.9 at 25°C and calculated using the following formula:

$$\text{Unit mg}^{-1} = \frac{\text{μmoles of maltose released}}{\text{Enzyme in reaction mixture (mg)} \times 3 \text{ min}} \quad (4)$$

Enzymatic activity was also measured in presence of different GdnHCl concentrations. For experiments involving GdnHCl with or without calcium, enzyme solution was incubated with desired concentrations of GdnHCl with or without 2 mM $CaCl_2$ overnight. Specific activity of BLA at different GdnHCl concentrations was expressed as percentage (%) specific activity by taking the activity of BLA in the absence of GdnHCl as 100%.

3.2.9 Chemical modifications of BLA

3.2.9.1 Succinylation

Succinylation of BLA was carried out following the procedure described by Klotz (1967) with slight modification, using 100 molar excess of succinic anhydride over protein. Succinic anhydride (90 mg) dissolved in 1.0 ml of DMSO was added in aliquots to a constantly stirred protein solution (500 mg BLA in 50 ml of 0.06 M sodium phosphate buffer, pH 7.5) over a period of 15 minutes at 4°C. The pH of the reaction mixture was maintained in the range of 7.5–8.0 with 1 N NaOH and the reaction was continued for 1 hour. Upon completion of the reaction, the protein solution was extensively dialyzed against 0.02 M Tris-HCl buffer, pH 7.5 for 48 hours. The modified preparation was stored at 4°C.

3.2.9.2 Carbamylation

The method of Stark (1967) was used for carbamylation of BLA using 0.66 M potassium cyanate. To 62 ml of BLA solution (10 mg/ml) prepared in 0.06 M sodium phosphate buffer, pH 7.7, 4.5 g solid potassium cyanate was added slowly within a time period of 30 minutes at 4°C with continuous stirring. The reaction was allowed to run for 48 hours at 4°C while maintaining the pH of the reaction mixture around 7.7–8.0 by simultaneous addition of 0.2 M acetic acid. After completion of the reaction, the protein solution was extensively dialyzed against 0.02 M Tris-HCl buffer, pH 7.5 for 48 hours and the modified protein was stored at 4°C.

3.2.9.3 Guanidination

Guanidination of BLA was performed according to the method of Kimmel (1967) using 0.46 M O-methylisourea. About 5.2 g of solid O-methylisourea was dissolved in 4 ml of water and its pH was adjusted to 10.5 with 5 N NaOH. This solution was then added in aliquots to a continuously stirred protein solution (600 mg BLA dissolved in 60 ml of 0.2 M carbonate-bicarbonate buffer, pH 10.5) within 30 minutes at 4°C. The reaction was continued for 96 hours at 4°C and the pH of the reaction mixture was maintained at 10.5 using 5 N NaOH. After completion of the reaction, the protein solution was extensively dialyzed against 0.02 M Tris-HCl buffer, pH 7.5 for 48 hours and the modified protein was stored at 4°C.

3.2.10 Quantification of modification

The percentage of modification was determined by TNBSA reaction following the method of Habeeb (1966) as described in the Pierce Chemical Bulletin. Different volumes (0.05–0.50 ml) of stock protein solution (400 µg/ml) were taken into different tubes and the volume in each tube was made to 0.50 ml with 0.1 M sodium bicarbonate

buffer, pH 8.5 if required. Then 0.25 ml of 0.01% (w/v) TNBSA solution was added into each tube and vortexed for homogeneous mixing. After 2 hours of incubation at 37°C, 0.25 ml of 10% (w/v) SDS solution was added to each tube followed by the addition of 0.125 ml of 1 N HCl with proper mixing. Absorbance of the yellow-colored derivative formed in the reaction was measured at 335 nm against a suitable blank. Data was plotted as absorbance at 335 nm versus amount of protein in mg and a straight line was drawn using least squares analysis. Slope values obtained with native and modified BLA preparations were used to calculate the percentage of modification using the formula given below:

$$\% \text{ Modification} = 1 - (m / m_o) \times 100 \quad (5)$$

where m is the slope value of the straight line obtained with modified BLA and m_o is the slope value obtained with native BLA.

3.2.11 Polyacrylamide gel electrophoresis

The charge homogeneity of native BLA and its modified derivatives was checked on 10% (w/v) polyacrylamide gel using tris-glycine buffer containing 0.025 M tris and 0.192 M glycine, pH 8.3 according to the method of Laemmli (1970) under non-denaturing conditions. Following solutions were used to prepare both stacking and resolving gels.

Solution A : 29.2% (w/v) Acrylamide and 0.8% (w/v) N,N'-methylenebisacrylamide

Solution B : 1.5 M Tris-HCl buffer, pH 8.8

Solution C : 10% (w/v) Ammonium persulfate

Solution D : 0.5 M Tris-HCl buffer, pH 8.8

Sample buffer : 62 mM Tris-HCl buffer, pH 6.8 containing 10% (v/v) glycerol and 0.001% (w/v) bromophenol blue

Electrophoresis buffer: Tris-glycine buffer containing 0.025 M tris and 0.192 M glycine, pH 8.3

Fixing solution : 40% (v/v) Methanol and 10% (v/v) acetic acid in water

Staining solution : 0.2% (w/v) Coomassie brilliant blue R-250 in fixing solution

Destaining solution : 7% (v/v) Acetic acid and 20% (v/v) methanol in water

Resolving gel was prepared by sequential mixing of 6.0 ml of solution A, 6.0 ml of solution B, 6.0 ml of water, 0.1 ml of solution C and 10 µl of TEMED. This solution was poured gently into the space between the glass plates assembled in the gel casting unit up to $3/4^{th}$ of their height. Subsequently, a layer of water was added on top of the resolving gel solution and the gel was allowed to polymerize at room temperature for 40 minutes. Meanwhile, stacking gel was prepared by mixing 1.4 ml of solution A, 2.5 ml of solution D, 6.1 ml of water, 0.2 ml of solution C and 10 µl of TEMED. After polymerization of the resolving gel, water layer from its top was removed with the help of filter paper strips. Then stacking gel solution was poured gently at the top of the resolving gel up to a height of 2.0 cm with the help of a micropipette. A comb was inserted into it and left for 1 hour at room temperature for polymerization. After 1 hour, the comb was removed from the stacking gel and the newly-formed wells were rinsed three times with electrophoresis buffer. Then glass plates with the polymerized gel were fitted into the electrophoresis apparatus half-filled with the electrophoresis buffer.

About 50 µg of native and modified BLA preparations were dissolved in 100 µl of the sample buffer and 10 µl (5 µg) of each preparation was loaded into different wells. The

remaining space of each well and the tank were filled with the electrophoresis buffer followed by covering of the tank with the lid containing electrode. The whole apparatus was connected to a power supply and a current of 60 V (6 V per well) was passed initially till all the protein bands had entered into the resolving gel. Then the voltage was increased to 120 V (12 V per well) and electrophoresis was continued for 1.5 hours till the dye front reached near the bottom of the gel. Upon completion of the electrophoresis, current was stopped, gel was gently removed from the glass plates and placed in the fixing solution overnight. It was stained with the staining solution for 2 hours and destained repeatedly with the destaining solution until the background was clear.

3.2.12 Analytical gel chromatography

Analytical gel chromatography was carried out as described earlier (Tayyab et al.,1991) using a Sephacryl S-200 HR column (1.63 × 56 cm) equilibrated with 0.02 M Tris-HCl buffer, pH 7.5 containing 0.02% (w/v) sodium azide. A glass column was washed with detergent, chromic acid and finally with water and mounted in a vibration-free position on a retort stand with the help of clamps. Its radius was determined by placing three strips of 3 cm each at three different places along the height of the column which was filled with water. Water equivalent to 3 cm height of the column was collected in three pre-weighed weighing bottles. Weight of water was obtained by subtracting the weight of empty bottles from the total weight of bottles containing water equivalent to 3 cm height of the column. Volume of water was obtained by dividing the weight of water by its density at room temperature. The radius of the column was obtained from the volume of water equivalent to 3 cm height of the column by using the following relationship:

$$V = \pi r^2 h \qquad (6)$$

where *V* is the volume of water collected in the weighing bottles, *r* is the radius of the column and *h* is 3 cm.

A small disc of glass wool, previously boiled in water was placed at the bottom of the column with the help of a glass rod. Few glass beads were added on the top of glass wool disc. The column was filled with water up to 1/4th of its total height. The pre-swollen Sephacryl S-200 HR gel was washed several times with water to remove fines and finally washed with the equilibration buffer (0.02 M Tris-HCl buffer, pH 7.5 containing 0.02% (w/v) sodium azide). The gel slurry was poured gently into the column through its sides using a glass rod and was allowed to settle under gravity for 6 hours. The upper buffer layer was removed by siphon and the remaining gel slurry was poured into the column after stirring the top layer of the gel with rubber tubing. The next day, the column was operated at a flow rate of 5 ml/hour which was increased slowly up to a flow rate of 20 ml/hour. The column bed was stabilized by passing equilibration buffer three times the total bed volume of the column. Void volume, V_o and inner volume, V_i of the column were determined by passing blue dextran (5 mg/2 ml) and L-tyrosine (2 mg/2 ml) respectively. The column was calibrated by passing different marker proteins (at least twice) with their Stokes radii in parentheses, namely cytochrome c (1.70 nm), α-chymotrypsinogen (2.24 nm), carbonic anhydrase (3.10 nm), BSA monomer (3.60 nm) and BSA dimer (4.30 nm) and their elution volumes (V_e) were determined. The mean values of their elution volumes were normalized in terms of distribution coefficient, K_d and available distribution coefficient, K_{av} according to the formulae given below (Andrews, 1970).

$$K_d = \frac{V_e - V_o}{V_i} \qquad (7)$$

$$K_{av} = \frac{V_e - V_o}{V_t - V_o} \quad (8)$$

where V_t is the total volume of the column.

Both native and modified BLA preparations were passed (two times) through the same column and their elution volumes were normalized into K_d and K_{av} in the same way as described for marker proteins.

3.2.13 Denaturation experiments

3.2.13.1 GdnHCl denaturation of native and Ca-depleted BLAs

GdnHCl denaturation of native and Ca-depleted BLAs in the absence and presence of 2 mM $CaCl_2$ were carried out in 0.02 M Tris-HCl buffer, pH 7.5 using CD and fluorescence measurements. All solutions were prepared in the same buffer. For experiments involving calcium, 2 mM $CaCl_2$ was included in all solutions.

Different stock protein solutions, 22.5 μM and 1.25 μM were prepared for experiments involving CD and fluorescence measurements respectively. To 0.4 ml of stock protein solution (final concentration = 1.8 μM for CD and 0.1 μM for fluorescence measurements) taken in different tubes, different volumes of buffer were added first followed by the addition of increasing volumes of stock GdnHCl solution (6.67 M) in order to obtain the desired denaturant concentration. The final incubation mixture (5.0 ml) was shaken well using a vortex mixer. The tubes were covered with a parafilm to prevent evaporation and incubated overnight at room temperature followed by CD and fluorescence measurements.

3.2.13.2 Urea denaturation of native, Ca-depleted and modified BLAs

Urea denaturation of native, Ca-depleted and modified BLAs were performed in 0.02 M Tris-HCl buffer, pH 7.5 using CD measurements. Native and Ca-depleted BLAs were also subjected to urea denaturation studies in the presence of 2 mM $CaCl_2$. For experiments involving calcium, 2 mM $CaCl_2$ was included in all solutions.

Different volumes of buffer were added to a constant volume (0.4 ml) of stock protein solution (final concentration = 1.8 μM) taken in different tubes. This was followed by the addition of increasing volumes of stock urea solution (10 M) to obtain the desired urea concentration in each tube. The contents of the incubation mixture (5.0 ml) were mixed well, covered with a parafilm and incubated overnight at room temperature. CD measurements were recorded in the far-UV range, 200–250 nm.

3.2.13.3 Data analysis

Analysis of urea denaturation data collected from CD measurements was carried out following a two-state model as described earlier (Muzammil et al., 2000). Relative MRE values at 222 nm obtained at different urea concentrations were transformed into F_D (apparent fraction of the denatured form) values using equation (9).

$$F_D = \frac{Y - Y_N}{Y_D - Y_N} \qquad (9)$$

where Y represents the MRE value at a given denaturant concentration and Y_N and Y_D are MRE values of the native and denatured states respectively, obtained by the linear extrapolation of pre- and post- transition zones. Values of F_D ranging from 0.2 to 0.8 were used to calculate the apparent equilibrium constant, K_D using the following equation (10).

$$K_D = \frac{F_D}{(1 - F_D)} \quad (10)$$

These K_D values were used to calculate the free energy change (ΔG_D) using equation (11).

$$\Delta G_D = - RT \ln K_D \quad (11)$$

where R is the gas constant (1.987 cal/deg/mol) and T is the absolute temperature (273 + 25°C). Free energy of stabilization, $\Delta G_D^{H_2O}$ was determined from the y-axis intercept of the linear plot of ΔG_D versus denaturant concentration [D] using least squares analysis which fitted the following equation (12).

$$\Delta G_D = \Delta G_D^{H_2O} - m[D] \quad (12)$$

where *m* is the slope value and is a measure of the dependence of ΔG_D on denaturant concentration.

CHAPTER 4

RESULTS

4.1 Effect of calcium on GdnHCl denaturation of native and Ca-depleted BLAs

GdnHCl denaturation of native and Ca-depleted BLAs was studied both in the absence and presence of 2 mM $CaCl_2$ using MRE, intrinsic fluorescence and activity as probes.

4.1.1 Circular dichroism

Denaturation of native and Ca-depleted BLAs was followed by ellipticity measurements at 222 nm with increasing GdnHCl concentrations both in the absence and presence of 2 mM $CaCl_2$. Ellipticity values were transformed into relative MRE at 222 nm as described in 'Materials and Methods' and plotted against GdnHCl concentration (Figures 4.1 and 4.2). As can be seen from Figure 4.1, native BLA showed a significant decrease in MRE (~54%) at 2.0 M GdnHCl compared to native protein. It should be noted that MRE data could not be collected at GdnHCl concentrations <2.0 M due to significant precipitation. A further decrease of ~14% in MRE was noted in the GdnHCl concentration range, 2.0–3.5 M. However, beyond 3.5 M GdnHCl, a gradual increase of ~25% in MRE was noted up to 6.0 M GdnHCl. Interestingly, addition of 2 mM $CaCl_2$ in the incubation mixture resulted in an increase in MRE values (compared to those observed in the absence of 2 mM $CaCl_2$) at all the GdnHCl concentrations used. Furthermore, MRE value remained constant within the GdnHCl concentration range, 1.5–5.5 M which was ~34% lesser than the MRE observed with the native protein. Previously observed precipitation at lower GdnHCl concentrations (<2.0 M) was also eliminated in the presence of 2 mM $CaCl_2$. Native commercial preparation was treated with 20 mM EGTA to remove bound calcium from the protein in order to obtain Ca-depleted BLA. Figure 4.2 shows GdnHCl denaturation profile of Ca-depleted BLA both

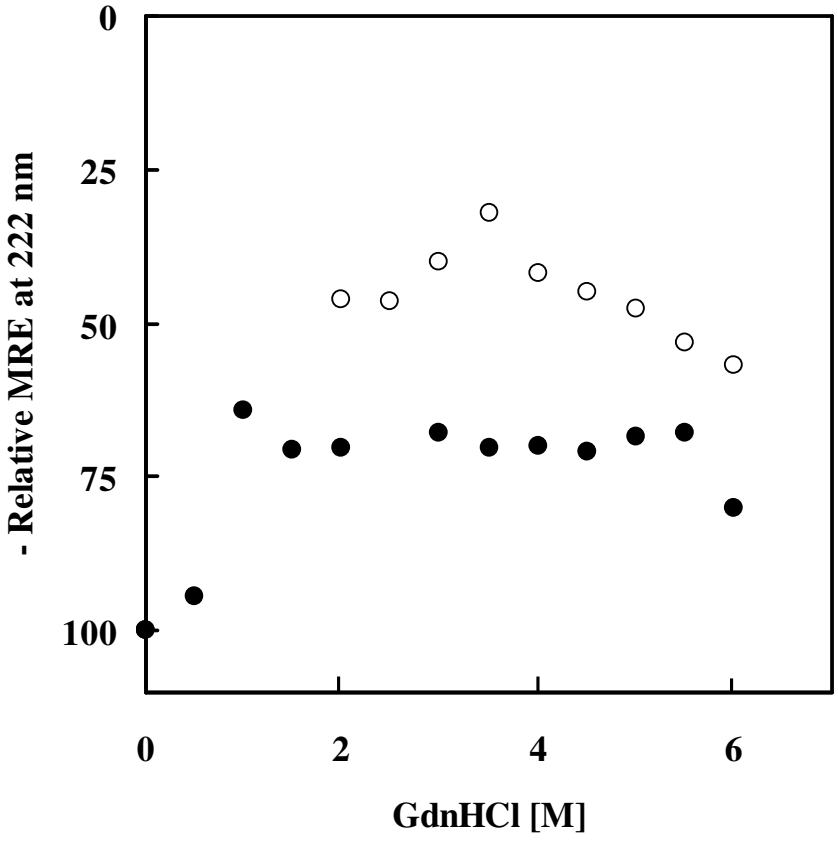

Figure 4.1: GdnHCl denaturation of native BLA in 0.02 M Tris-HCl buffer, pH 7.5 in the absence (○) and presence (●) of 2 mM $CaCl_2$ as followed by MRE measurements at 222 nm. CD data were transformed into relative MRE as described in 'MATERIALS AND METHODS' and plotted against GdnHCl concentration.

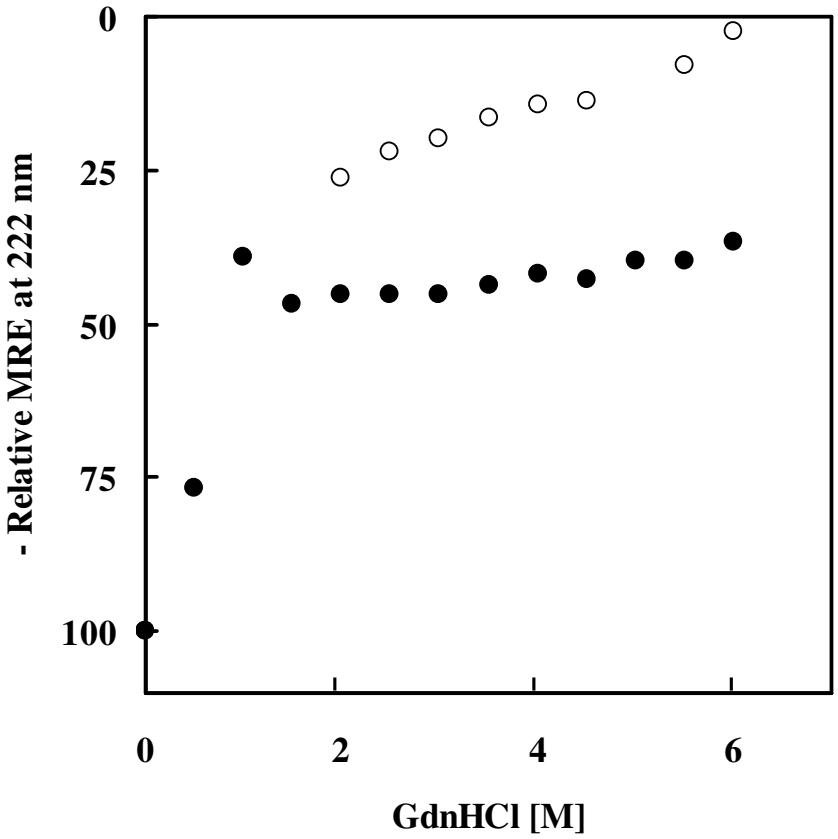

Figure 4.2: GdnHCl denaturation of Ca-depleted BLA in 0.02 M Tris-HCl buffer, pH 7.5 in the absence (○) and presence (●) of 2 mM $CaCl_2$ as followed by MRE measurements at 222 nm. CD data were transformed into relative MRE and plotted against GdnHCl concentration.

in the absence and presence of 2 mM $CaCl_2$. Ca-depleted BLA also showed precipitation in the lower GdnHCl concentration range *i.e.* <2.0 M. Therefore, denaturation was studied in the GdnHCl concentration range, 2.0–6.0 M in the absence of 2 mM $CaCl_2$. A marked reduction in MRE (~74%) was observed at 2.0 M GdnHCl compared to the value obtained in the absence of GdnHCl. There was a gradual decrease in MRE from ~26% at 2.0 M GdnHCl to ~2% at 6.0 M GdnHCl (Figure 4.2). Presence of 2 mM $CaCl_2$ in the incubation mixture produced significant reversal in MRE values which was more or less the same as reflected from the similar values of MRE within GdnHCl concentration range, 1.5–6.0 M.

4.1.2 Intrinsic fluorescence

The effect of calcium on GdnHCl-induced denaturation of BLA was studied by detecting fluorescence signals upon excitation at 280 nm. The observed emission spectrum of native BLA showed an emission maximum at 336 nm. Figure 4.3 shows the effect of increasing GdnHCl concentrations on the relative fluorescence intensity of native BLA at 336 nm in the absence and presence of 2 mM $CaCl_2$ when excited at 280 nm. As can be seen from the figure, a significant decrease (~ 38%) in fluorescence intensity of native BLA was observed up to 1.0 M GdnHCl in the absence of 2 mM $CaCl_2$. This decrease in fluorescence intensity remained constant up to 4.0 M GdnHCl. Increasing GdnHCl concentrations beyond 4.0 M led to a gradual increase in fluorescence intensity reaching ~88% at 6.0 M GdnHCl. On the other hand, fluorescence intensity signal showed smaller variation (~7%) in the presence of 2 mM $CaCl_2$ throughout the concentration range of GdnHCl used (Figure 4.3). In other words, decrease in fluorescence intensity observed in the absence of 2 mM $CaCl_2$ was almost abolished upon addition of 2 mM $CaCl_2$. GdnHCl denaturation of Ca-depleted BLA both in the absence and presence of 2 mM $CaCl_2$ as monitored by fluorescence

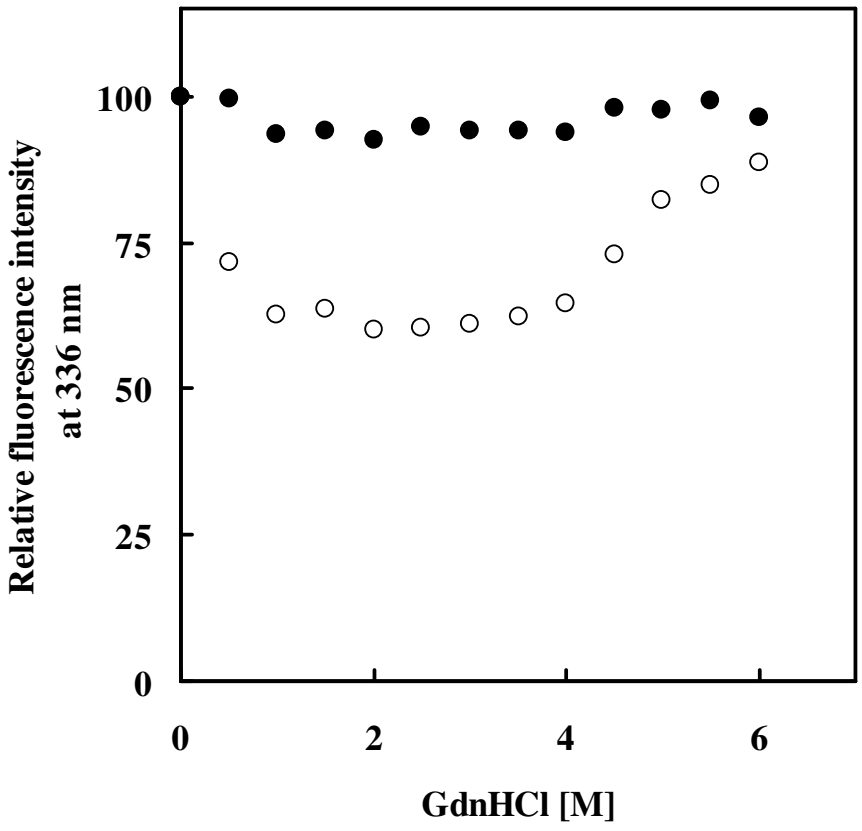

Figure 4.3: GdnHCl denaturation of native BLA in 0.02 M Tris-HCl buffer, pH 7.5 in the absence (○) and presence (●) of 2 mM $CaCl_2$ as followed by fluorescence measurements at 336 nm upon excitation at 280 nm. Fluorescence intensity data were transformed into relative fluorescence intensity as described in 'MATERIALS AND METHODS' and plotted against GdnHCl concentration.

intensity at its emission maximum (338 nm) is shown in Figure 4.4. A drastic decrease in relative fluorescence intensity (~57%) was observed at 1.0 M GdnHCl followed by a gradual increase in fluorescence intensity reaching to a value of ~63% at 6.0 M GdnHCl. Presence of 2 mM $CaCl_2$ in the incubation mixture produced a lesser decrease in fluorescence intensity at all GdnHCl concentrations used when compared to the values obtained in the absence of 2 mM $CaCl_2$. Specifically, the reversal in fluorescence intensity was more pronounced (~34%) at 0.5 M GdnHCl followed by ~15–20% at higher GdnHCl concentrations.

In addition to the change in relative fluorescence intensity observed with native BLA in the absence of 2 mM $CaCl_2$, emission maximum (336 nm) was also shifted (8 nm) towards higher wavelength (red shift) up to 3.5 M GdnHCl and reverted back to lower wavelength above 3.5 M GdnHCl (Figure 4.5). At 6.0 M GdnHCl, emission maximum of native BLA was found to be at 337 nm. Presence of 2 mM $CaCl_2$ in the reaction mixture abolished this effect as emission maximum remained indifferent (within experimental error) throughout the GdnHCl concentration range (Figure 4.5). This behavior of shift in emission maximum in the absence of 2 mM $CaCl_2$ and its abolishment upon addition of 2 mM $CaCl_2$ was similar to the pattern of relative fluorescence intensity signal shown in Figure 4.3. The shift in emission maximum was also observed with Ca-depleted BLA upon GdnHCl denaturation (Figure 4.6). Similar red shift of 8 nm was observed at 3.5 M GdnHCl which was reduced to 5 nm at 6.0 M GdnHCl. Addition of 2 mM $CaCl_2$ though significantly reduced the extent of red shift at all GdnHCl concentrations but failed to abolish the shift in emission maximum completely as observed with native BLA in presence of 2 mM $CaCl_2$ (Figure 4.5).

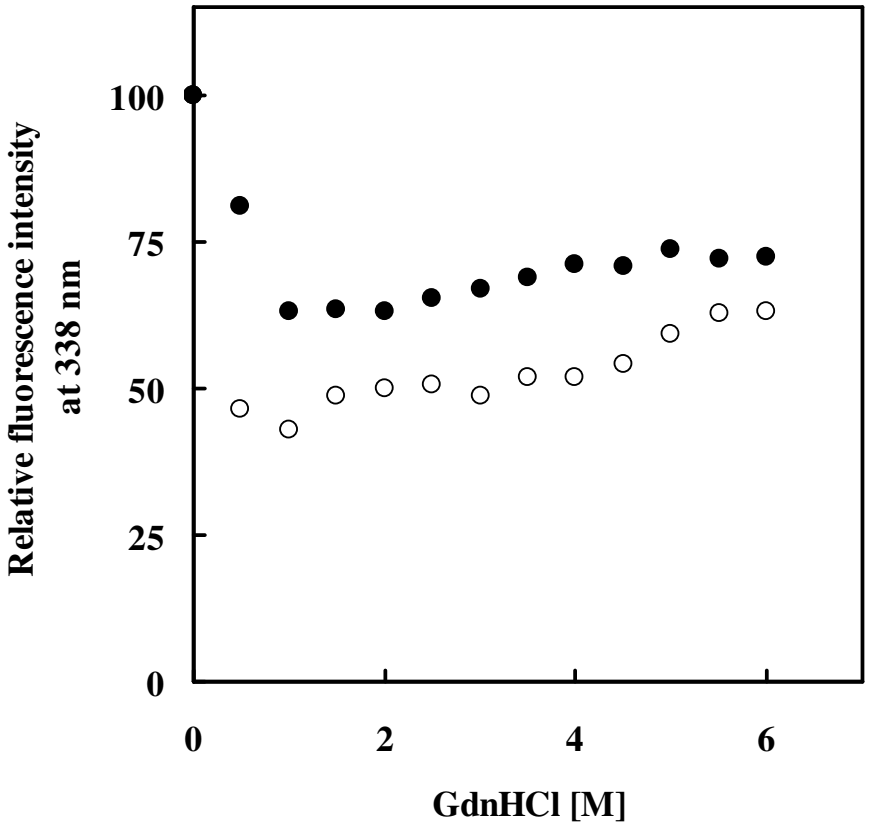

Figure 4.4: GdnHCl denaturation of Ca-depleted BLA in 0.02 M Tris-HCl buffer, pH 7.5 in the absence (○) and presence (●) of 2 mM $CaCl_2$ as followed by fluorescence measurements at 338 nm upon excitation at 280 nm. Fluorescence intensity data were transformed into relative fluorescence intensity and plotted against GdnHCl concentration.

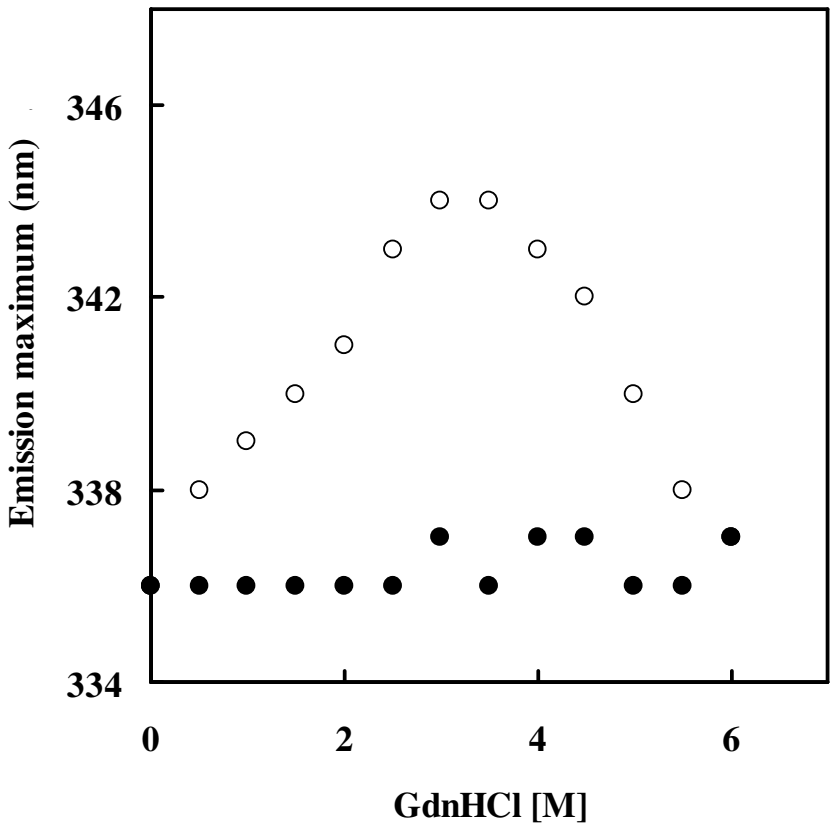

Figure 4.5: GdnHCl denaturation of native BLA in 0.02 M Tris-HCl buffer, pH 7.5 in the absence (○) and presence (●) of 2 mM $CaCl_2$ as followed by change in emission maximum upon excitation at 280 nm. Variation in emission maximum of native BLA was plotted against GdnHCl concentration.

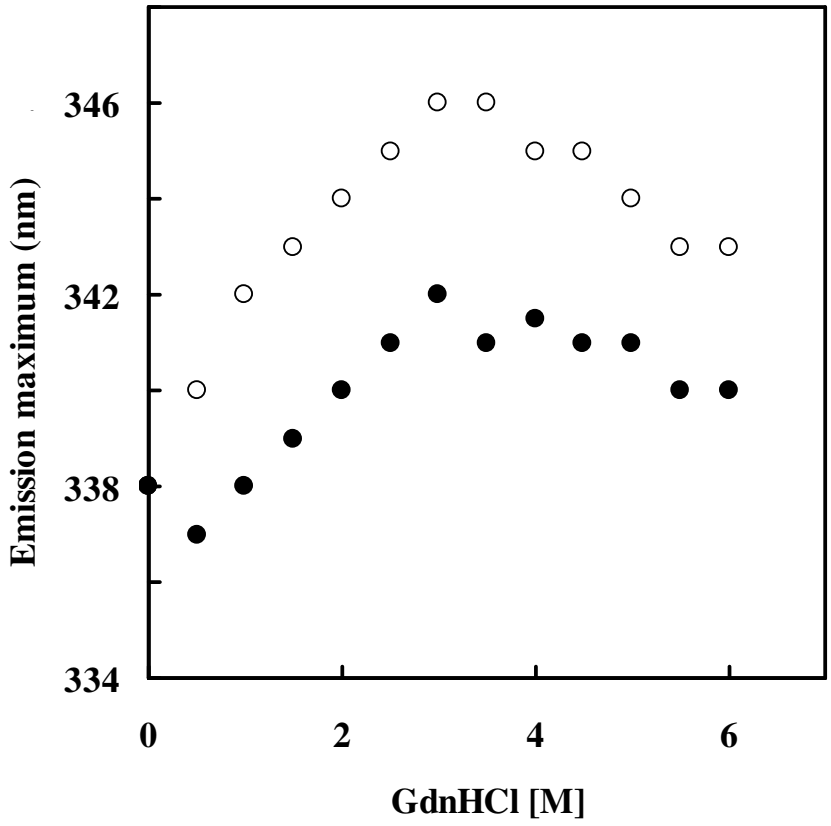

Figure 4.6: GdnHCl denaturation of Ca-depleted BLA in 0.02 M Tris-HCl buffer, pH 7.5 in the absence (○) and presence (●) of 2 mM $CaCl_2$ as followed by change in emission maximum upon excitation at 280 nm. Variation in emission maximum of Ca-depleted BLA was plotted against GdnHCl concentration.

4.1.3 Enzymatic activity

Enzymatic activity of BLA in presence of different GdnHCl concentrations with and without 2 mM $CaCl_2$ was measured to investigate the effect of GdnHCl on its biological activity. Figures 4.7 and 4.8 show the effect of increasing GdnHCl concentrations on the enzymatic activity of native and Ca-depleted BLAs both in the absence and presence of 2 mM $CaCl_2$. About 85% loss in enzymatic activity of native BLA was observed at 1.0 M GdnHCl in the absence of 2 mM $CaCl_2$ (Figure 4.7), which remained constant up to 3.0 M and increased gradually thereafter, reaching ~31% activity (~69% loss) at 6.0 M GdnHCl. On the other hand, activity of native BLA in presence of 2 mM $CaCl_2$ showed relatively lesser loss at all GdnHCl concentrations used. For example, ~25 % loss in enzymatic activity was observed at 1.0 M GdnHCl concentration in presence of 2 mM $CaCl_2$. There was a gradual decrease in enzymatic activity with increasing GdnHCl concentrations reaching to a value of ~46% (~54% decrease) at 6.0 M GdnHCl (Figure 4.7). Effect of GdnHCl on the activity of Ca-depleted BLA both in the absence and presence of 2 mM $CaCl_2$ is shown in Figure 4.8. A complete loss of enzymatic activity was observed at 1.0 M GdnHCl for Ca-depleted BLA in the absence of 2 mM $CaCl_2$, which persisted throughout the GdnHCl concentrations used. A relatively higher percentage of enzymatic activity was observed in the whole GdnHCl concentration range in the presence of 2 mM $CaCl_2$. Even at 6.0 M GdnHCl, about 14% activity was retained.

4.2 Chemical modifications of lysine residues of BLA

Figure 4.9 shows the results of TNBSA color reaction with native (N), succinylated (S), carbamylated (C) and guanidinated (G) BLAs, prepared by treating native BLA with succinic anhydride, potassium cyanate and O-methylisourea hydrogen sulfate respectively, under given reaction conditions (Table 4.1). A linear increase in

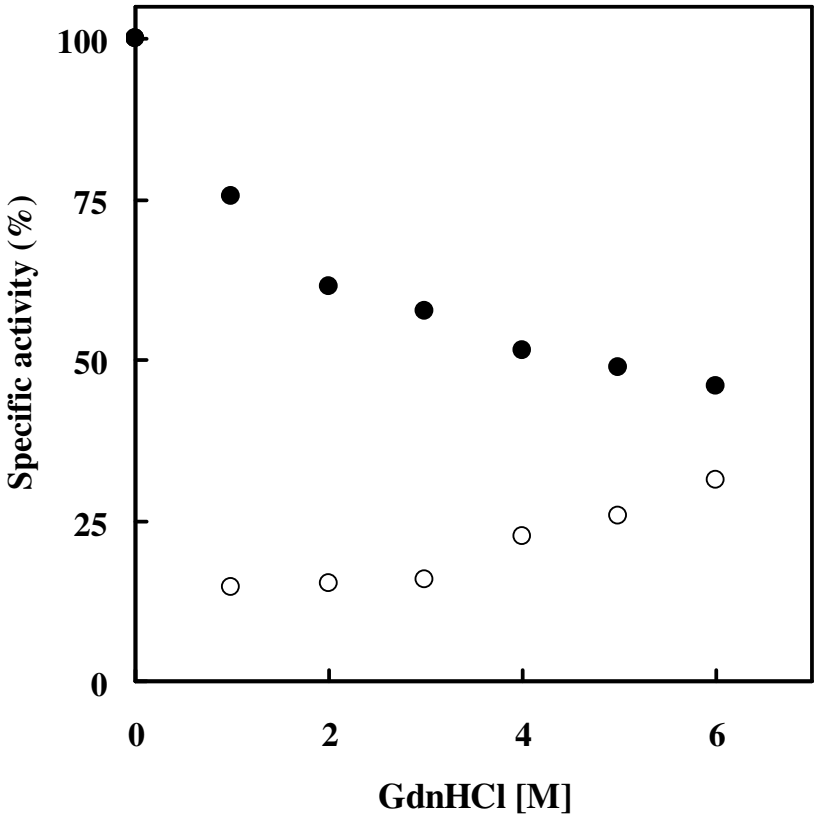

Figure 4.7: Effect of increasing GdnHCl concentrations on the specific activity of native BLA in the absence (○) and presence (●) of 2 mM $CaCl_2$. Specific activity of native BLA was transformed into percentage specific activity and plotted against GdnHCl concentration.

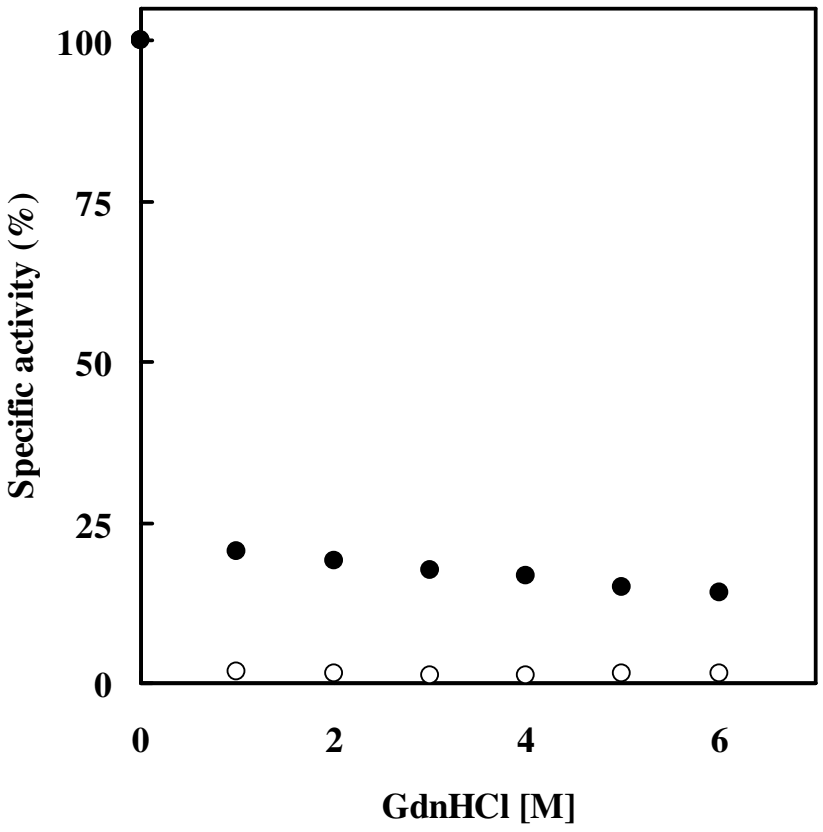

Figure 4.8: Effect of increasing GdnHCl concentrations on the specific activity of Ca-depleted BLA in the absence (○) and presence (●) of 2 mM $CaCl_2$. Specific activity of Ca-depleted BLA was transformed into percentage specific activity and plotted against GdnHCl concentration.

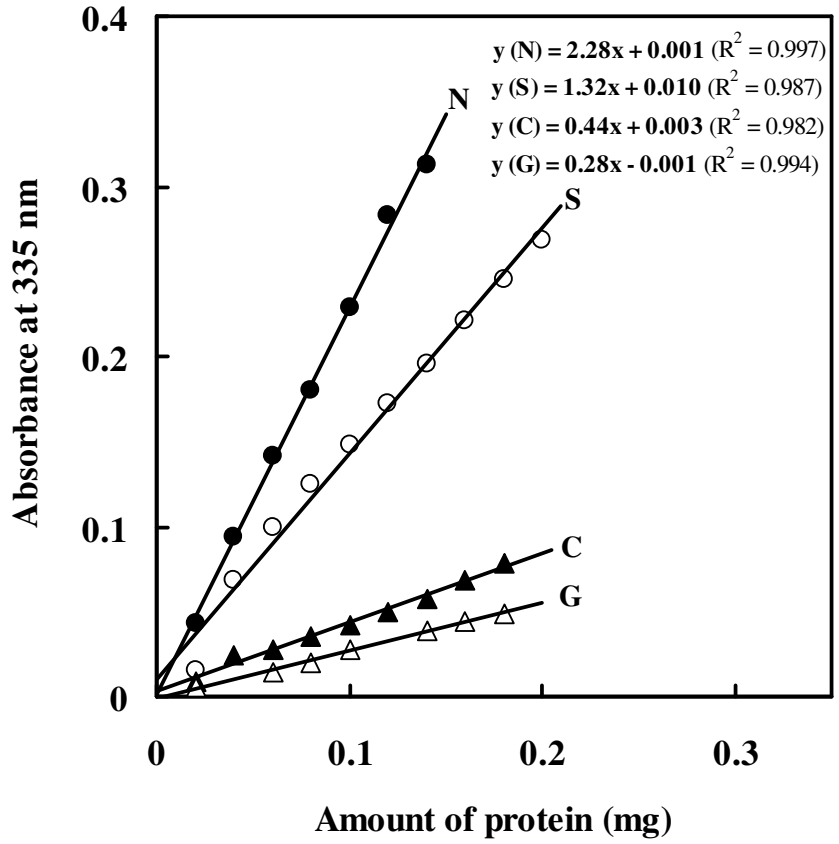

Figure 4.9: TNBSA color reaction to determine the extent of modification in succinylated, carbamylated and guanidinated BLA preparations. Symbols 'N' (●), 'S' (○), 'C' (▲) and 'G' (Δ) refer to native, succinylated, carbamylated and guanidinated BLA preparations respectively. Straight lines were drawn using least squares analysis.

Table 4.1: Chemical modifications of amino groups of BLA.

BLA preparations	**Reaction conditions**	**Slope of TNBSA color reaction**	**Extent of modification (%)**	**No. of amino groups modified***	**Relative mobility (R_m)**
Native	–	2.28	0	0	0.09
Succinylated	100 Molar excess of succinic anhydride, 1 h, pH 7.5, 4°C	1.32	42	12	0.47
Carbamylated	0.66 M Potassium cyanate, 48 h, pH 7.7–8.0, 4°C	0.44	81	24	0.47
Guanidinated	0.46 M O-methylisourea, 96 h, pH 10.5, 4°C	0.28	88	26	0.06

*Total number of amino groups was taken as 29 (1 α-amino + 28 ε-amino groups) (Tomazic & Klibanov, 1988).

absorbance at 335 nm was observed upon increasing protein concentration in all preparations. However, modified preparations showed reduction in the slope value which was more pronounced in carbamylated and guanidinated BLAs (Figure 4.9, Table 4.1). Quantification of modification of amino groups of BLA in modified preparations resulted in the percentage of modification as 42%, 81% and 88% for succinylated, carbamylated and guanidinated preparations respectively (Table 4.1).

Charge homogeneity of native and modified BLAs was checked by polyacrylamide gel electrophoresis (PAGE) at pH 8.3, according to the method of Laemmli (1970). Figure 4.10 shows the electrophoretic pattern of native (N), 42% succinylated (S_{42}), 81% carbamylated (C_{81}) and 88% guanidinated (G_{88}) BLAs on 10% polyacrylamide gel. All these preparations produced a single band with different anodic mobilities. Both S_{42} and C_{81} BLA preparations showed higher anodic mobilities (0.47) compared to 0.09 obtained with native BLA (Table 4.1). On the other hand, G_{88} preparation showed lesser deviation in relative mobility (0.06) compared to native BLA. Native and modified BLA preparations were also eluted from a Sephacryl S-200 HR column (1.63×56 cm) in the form of a single symmetrical peak as shown in Figures 4.11 – 4.13.

4.3 Conformational changes in modified BLAs

Stokes radii of native and modified BLAs were determined by analytical gel chromatography on a calibrated Sephacryl S-200 HR column (1.63×56 cm) equilibrated with 0.02 M Tris-HCl buffer, pH 7.5 in order to examine the conformational changes (if any) in BLA upon modifications of lysine residues. Void volume, V_o and inner volume, V_i of the column were determined to be 46.5 and 69.0 ml respectively whereas different marker proteins had elution volumes of 114.0, 90.5, 71.0, 58.0 and 52.0 ml for cytochrome c, α-chymotrypsinogen A, carbonic anhydrase, BSA monomer and BSA

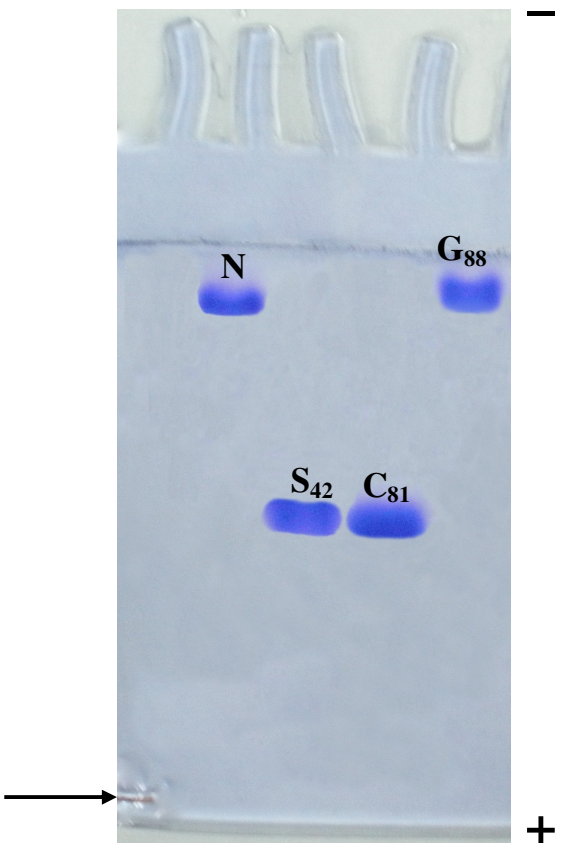

Figure 4.10: PAGE pattern of native (N), 42% succinylated (S_{42}), 81% carbamylated (C_{81}) and 88% guanidinated (G_{88}) BLA preparations on 10% polyacrylamide gel performed according to Laemmli (1970) under non-denaturing condition. Arrow at the bottom shows the position of tracking dye.

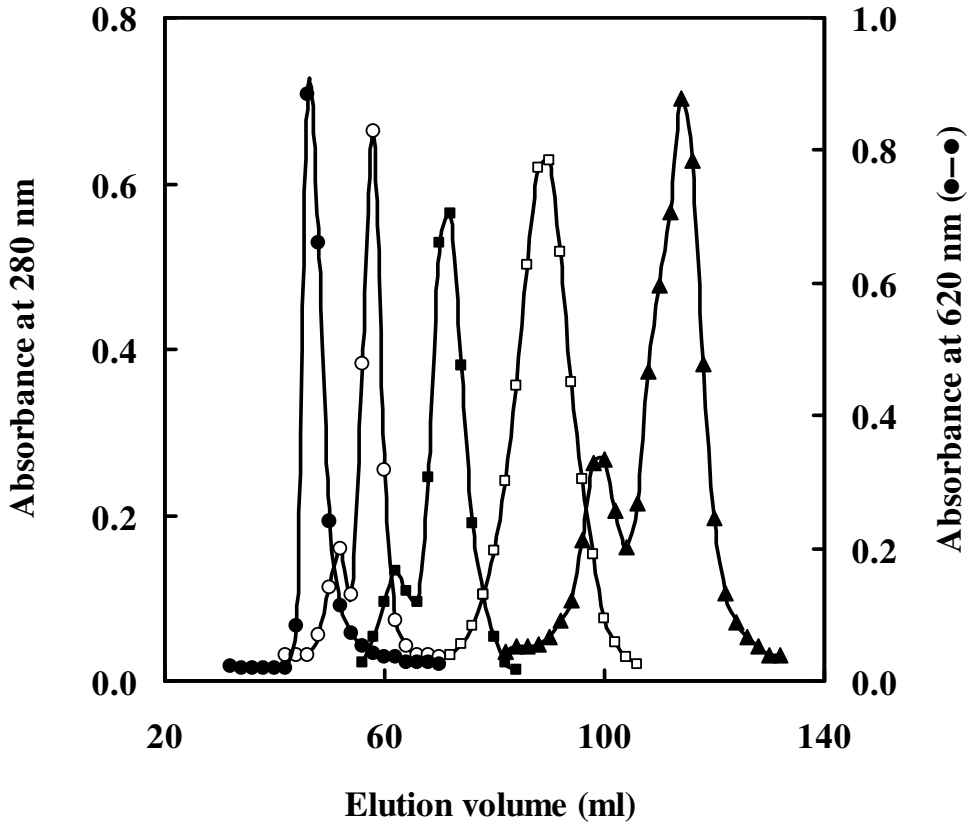

Figure 4.11: Elution profiles of blue dextran (●), BSA monomer (○), carbonic anhydrase (■), native BLA (□) and cytochrome c (▲) on Sephacryl S-200 HR column (1.63×56 cm) equilibrated with 0.02 M Tris-HCl buffer, pH 7.5 containing 0.02% sodium azide. Different amount of proteins *i.e.* ~3 mg (native BLA and carbonic anhydrase), ~5 mg (BSA) and 10 mg (cytochrome c), dissolved in the same buffer were loaded on to the column and eluted with a flow rate of 15 ml/hour. Fractions of 2 ml were collected and monitored for protein by taking the absorbance at 280 nm. For blue dextran, the sample size was 5 mg/2 ml of the same buffer and fractions were monitored by taking the absorbance at 620 nm.

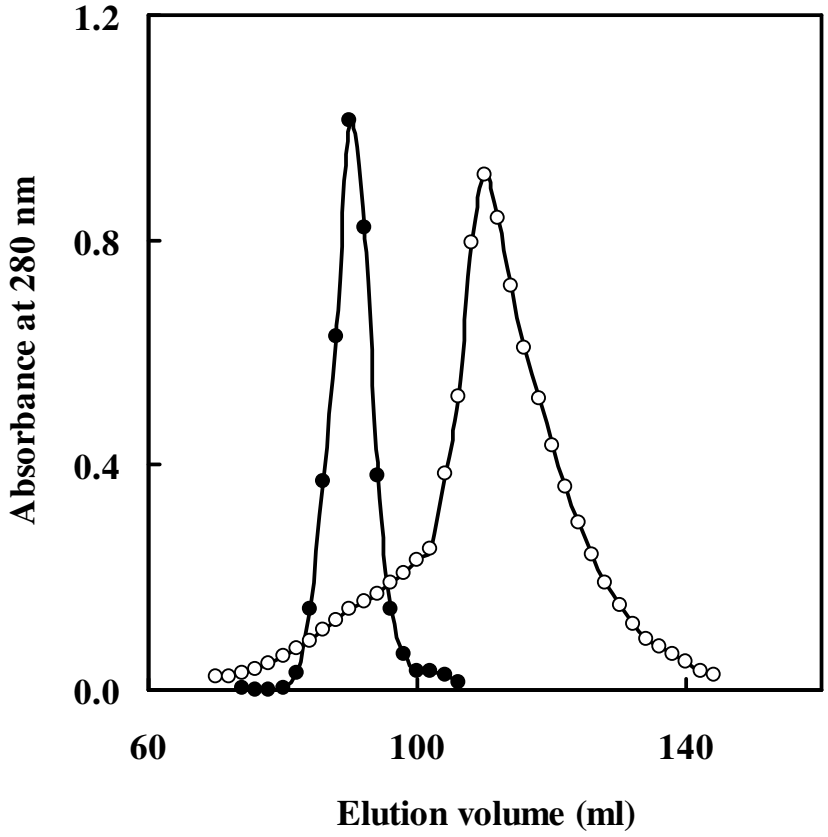

Figure 4.12: Elution profiles of α-chymotrypsinogen A (●) and G_{88} BLA (○) on Sephacryl S-200 HR column (1.63×56 cm) equilibrated with 0.02 M Tris-HCl buffer, pH 7.5 containing 0.02% sodium azide. Proteins with a sample size of ~4 mg for α-chymotrypsinogen A and ~7 mg for G_{88} BLA in 2 ml of the above buffer were loaded on to the column and eluted with a flow rate of 15 ml/hour. Fractions of 2 ml were collected and monitored for protein by taking the absorbance at 280 nm.

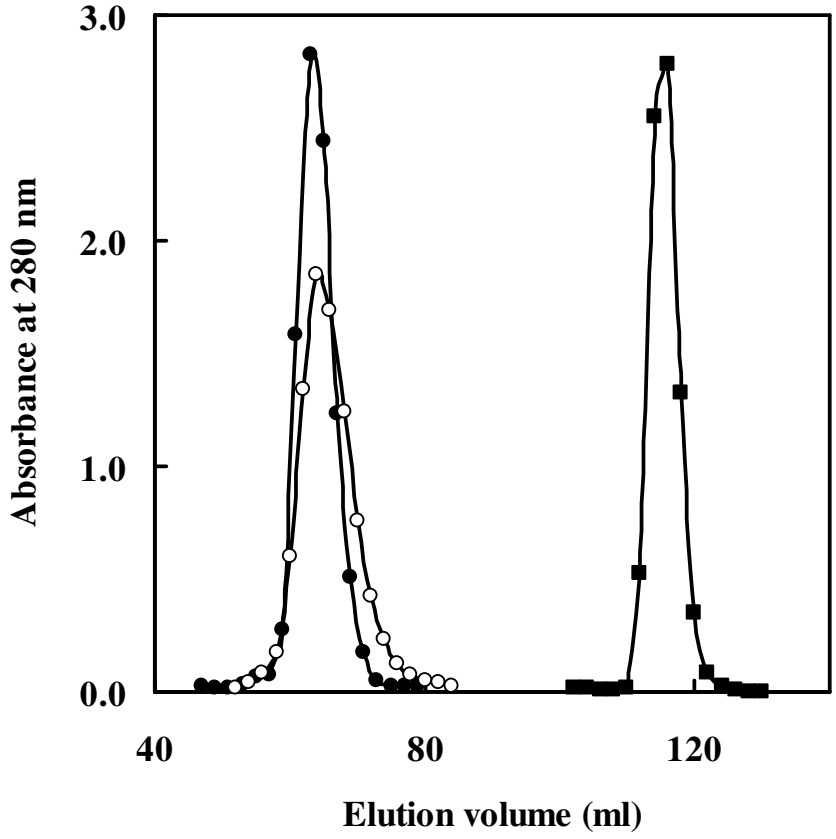

Figure 4.13: Elution profiles of C_{81} BLA (●), S_{42} BLA (○) and L-tyrosine (■) on Sephacryl S-200 HR column (1.63×56 cm) equilibrated with 0.02 M Tris-HCl buffer, pH 7.5 containing 0.02% sodium azide. Proteins with a sample size of ~7–8 mg per 2 ml of the above buffer were loaded on to the column and eluted with a flow rate of 15 ml/hour. Fractions of 2 ml were collected and monitored for protein by taking the absorbance at 280 nm. The sample size of L-tyrosine was 2 mg/2 ml of the same buffer and fractions were monitored by taking the absorbance at 280 nm.

dimer respectively (Figures 4.11–4.13, Table 4.2). Elution profiles of native, S_{42}, C_{81} and G_{88} BLAs are also shown in Figures 4.11–4.13 where each of these proteins except G_{88} BLA eluted in the form of single symmetrical peak. G_{88} BLA showed trailing on the ascending limb of the elution profile. As can be seen from the figures, both succinylated and carbamylated BLA preparations eluted much earlier with elution volumes of 65 and 63 ml for S_{42} and C_{81} BLAs respectively as opposed to 89 ml, obtained for native BLA (Table 4.2). On the other hand, the elution volume (110.0 ml) of guanidinated BLA preparation was found to be much higher than that of native BLA (Table 4.2). Values of elution volume of marker proteins, native, S_{42}, C_{81} and G_{88} BLA preparations were transformed into K_d, K_{av}, $(-\log K_{av})^{1/2}$ and $\text{erfc}^{-1}K_d$ values according to standard procedures as described in Materials and Methods (Table 4.2). Figures 4.14 and 4.15 show linear plots drawn following the methods of Ackers (1967) and Laurent & Killander (1964) respectively, which yielded the following straight line equations.

$$\text{Stokes radius, nm} = 2.13\ \text{erfc}^{-1}K_d + 1.61 \qquad (13)$$

$$(-\log K_{av})^{1/2} = 0.34\ \text{Stokes radius, nm} - 0.38 \qquad (14)$$

Substitution of $\text{erfc}^{-1}K_d$ and $(-\log K_{av})^{1/2}$ values of native, S_{42}, C_{81} and G_{88} BLAs into equations (13) and (14) yielded Stokes radii of these preparations which along with the mean values are shown in Table 4.3. Stokes radii of S_{42} and C_{81} BLAs were found to be higher than native BLA while G_{88} showed a decrease in Stokes radius.

4.4 Conformational stabilities of native, Ca-depleted and modified BLAs

Figures 4.16 and 4.17 show urea-induced denaturation of native and Ca-depleted BLAs as followed by MRE measurements at 222 nm. In order to rule out the effect of

Table 4.2: Analytical gel chromatographic data of marker proteins, native and modified BLAs on Sephacryl S-200 HR column (1.63 × 56 cm) at pH 7.5.

Proteins	**V_e (ml)**	**K_d**	**K_{av}**	**$(-\log K_{av})^{1/2}$**	**$erfc^{-1} K_d$**
BSA dimer	52.0	0.080	0.078	1.053	1.237
BSA monomer	58.0	0.167	0.163	0.887	0.979
Carbonic anhydrase	71.0	0.355	0.348	0.678	0.656
α-Chymotrypsinogen	90.5	0.638	0.624	0.453	0.332
Cytochrome c	114.0	0.978	0.957	0.138	0.020
Native	89.0	0.616	0.603	0.469	0.355
S_{42}	65.0	0.261	0.255	0.770	0.798
C_{81}	63.0	0.242	0.237	0.791	0.829
G_{88}	110.0	0.920	0.901	0.213	0.071

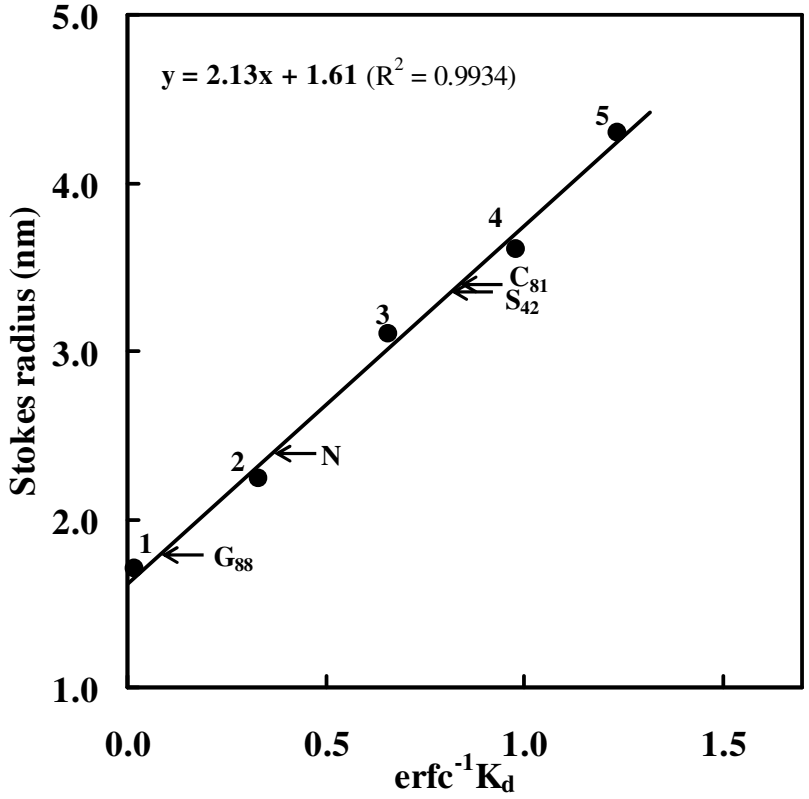

Figure 4.14: Stokes' radii determination of native (N), 42% succinylated (S_{42}), 81% carbamylated (C_{81}) and 88% guanidinated (G_{88}) BLAs according to Ackers (1967). Numbers 1-5 refer to different marker proteins: 1. cytochrome c; 2. α-chymotrypsinogen A; 3. carbonic anhydrase; 4. BSA monomer and 5. BSA dimer. Positions of native (N) and modified (S_{42}, C_{81} and G_{88}) BLAs are shown by arrows. Straight line was drawn using least squares analysis.

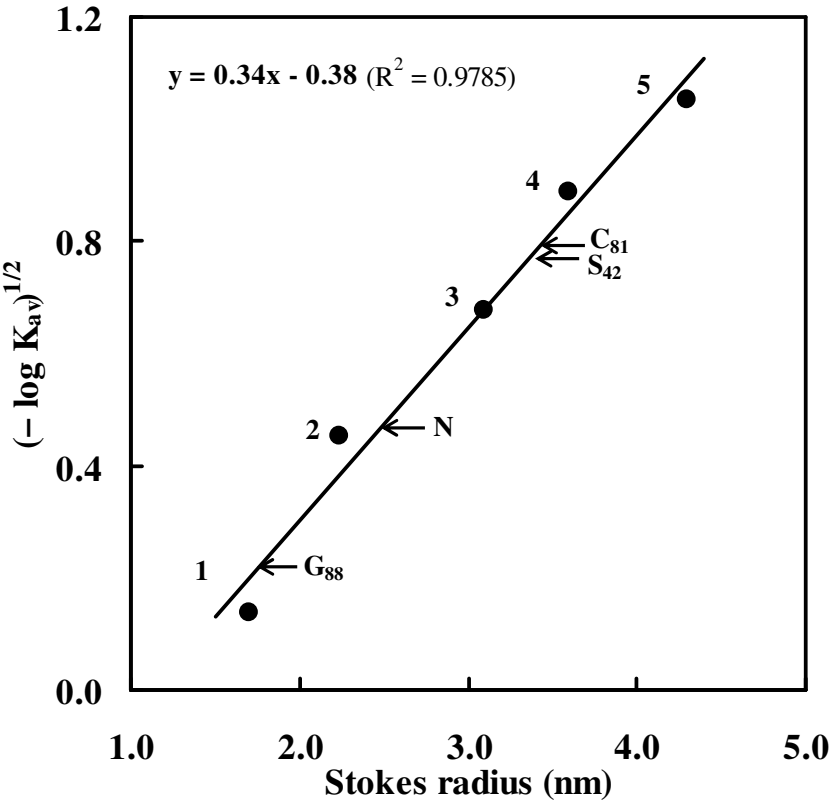

Figure 4.15: Stokes' radii determination of native (N), 42% succinylated (S_{42}), 81% carbamylated (C_{81}) and 88% guanidinated (G_{88}) BLAs according to Laurent and Killander (1964). Numbers 1-5 refer to different marker proteins: 1. cytochrome c; 2. α-chymotrypsinogen A; 3. carbonic anhydrase; 4. BSA monomer and 5. BSA dimer. Positions of native (N) and modified (S_{42}, C_{81} and G_{88}) BLAs are shown by arrows. Straight line was drawn using least squares analysis.

Table 4.3: Stokes radii of native, 42% succinylated, 81% carbamylated and 88% guanidinated BLAs at pH 7.5.

BLA preparations	**Stokes radius (nm)**		
	From Eq. 1	**From Eq. 2**	**Mean**
Native	2.37	2.48	2.43
S_{42}	3.31	3.36	3.34
C_{81}	3.38	3.42	3.40
G_{88}	1.77	1.74	1.76

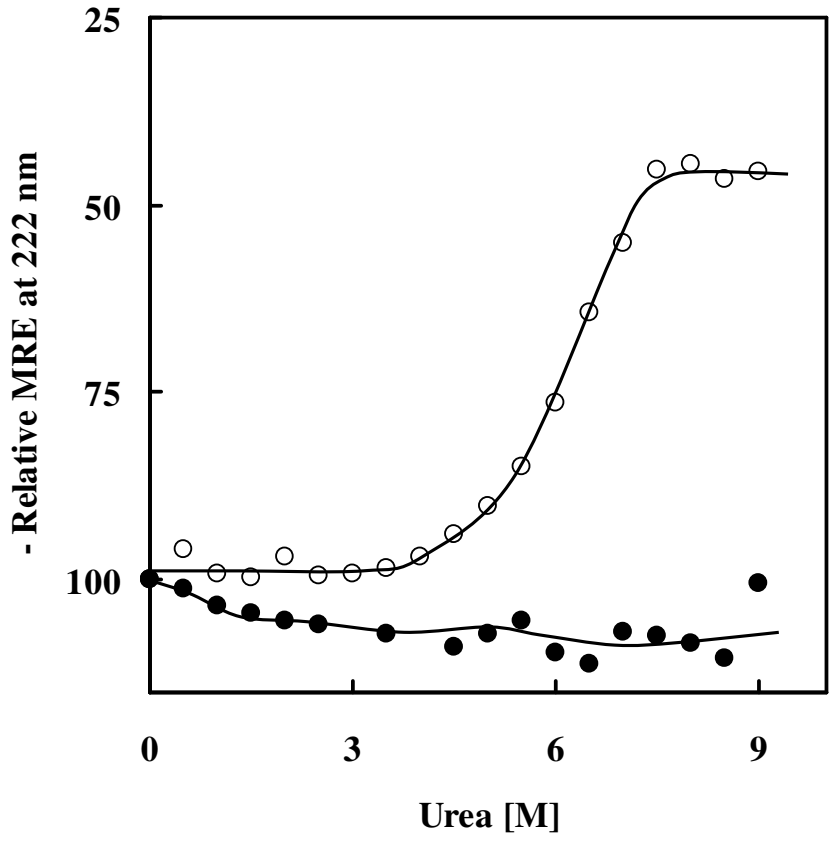

Figure 4.16: Plots of relative $MRE_{222\ nm}$ of native BLA in 0.02 M Tris-HCl buffer, pH 7.5 at 25°C versus urea concentration, in the absence (○) and presence (●) of 2 mM $CaCl_2$. Relative $MRE_{222\ nm}$ values at each urea concentration were calculated by taking the $MRE_{222\ nm}$ value of the native protein in the absence of urea as 100.

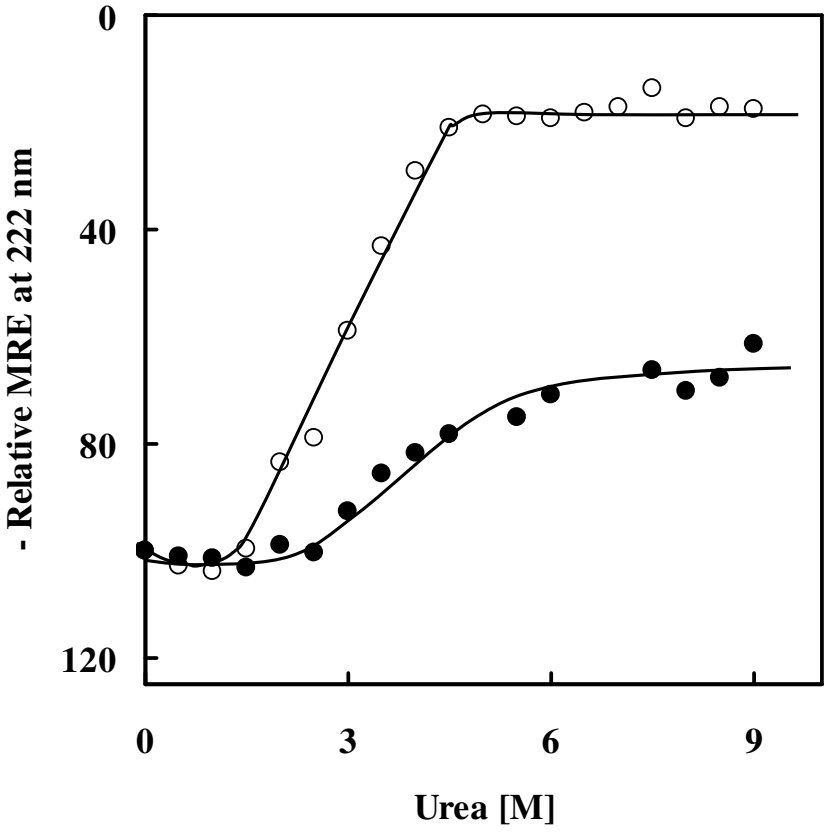

Figure 4.17: Plots of relative $MRE_{222\ nm}$ of Ca-depleted BLA in 0.02 M Tris-HCl buffer, pH 7.5 at 25°C versus urea concentration in the absence (○) and presence (●) of 2 mM $CaCl_2$. Relative $MRE_{222\ nm}$ values at each urea concentration were calculated by taking the $MRE_{222\ nm}$ value of Ca-depleted BLA in the absence of urea as 100.

concentration (if any), MRE values at 222 nm were transformed into relative MRE as described in 'MATERIALS AND METHODS' and plotted against urea concentration. As can be seen from the figure, there was a decrease in MRE value on increasing the urea concentration in both preparations being more pronounced and started earlier in Ca-depleted BLA compared to native BLA. Denaturation of both proteins followed a single-step, two-state transition model. The transition curve of Ca-depleted BLA started at 1.0 M urea concentration and completed at 4.5 M with a mid-point occurring at 3.25 M (Figure 4.17, Table 4.4). Furthermore, decrease in MRE value at the completion of transition was ~83%. In the presence of 2 mM $CaCl_2$, the transition curve of Ca-depleted BLA shifted towards right with a start-point at 2.5 M and ended around 6.0 M urea. On the other hand, transition curve of native BLA (partially saturated with calcium) had the characteristics of start-, mid- and end-points as 3.5, 6.25 and 7.5 M respectively (Figure 4.16, Table 4.4). No significant change in MRE values was observed in the presence of 2 mM $CaCl_2$ with native BLA preparation (Figure 4.16).

Similar single-step, two-state transitions were observed for all modified BLA preparations (Figures 4.18–4.20). However, their transitions differed significantly in terms of start-, mid- and end-points of transition. For example, urea transition of S_{42} BLA started at 2.5 M and ended at 7.5 M with a mid-point occurring at 5.0 M urea. On the other hand, urea transition of C_{81} BLA started and ended much earlier than the transition of S_{42} BLA at 1.0 M and 4.5 M respectively with the appearance of a mid-point at 3.25 M (Table 4.4). Meanwhile urea transition of G_{88} BLA started as early as C_{81} BLA at 1.0 M but with a later mid- and end-point at 4.25 and 5.5 M respectively (Table 4.4).

Table 4.4: Urea denaturation data of native, Ca-depleted, 42% succinylated, 81% carbamylated and 88% guanidinated BLAs at pH 7.5 as monitored by MRE measurements at 222 nm.

BLA preparations	**Transition**			$\Delta G_D^{H_2O}$ **(cal/mol)**
	Start-point [M]	**Mid-point [M]**	**End-point [M]**	
Native	3.50	6.25	7.50	5,930
Ca-depleted	1.00	3.25	4.50	3,430
S_{42}	2.50	5.00	7.50	3,957
C_{81}	1.00	3.25	4.50	3,336
G_{88}	1.00	4.25	5.50	3,383

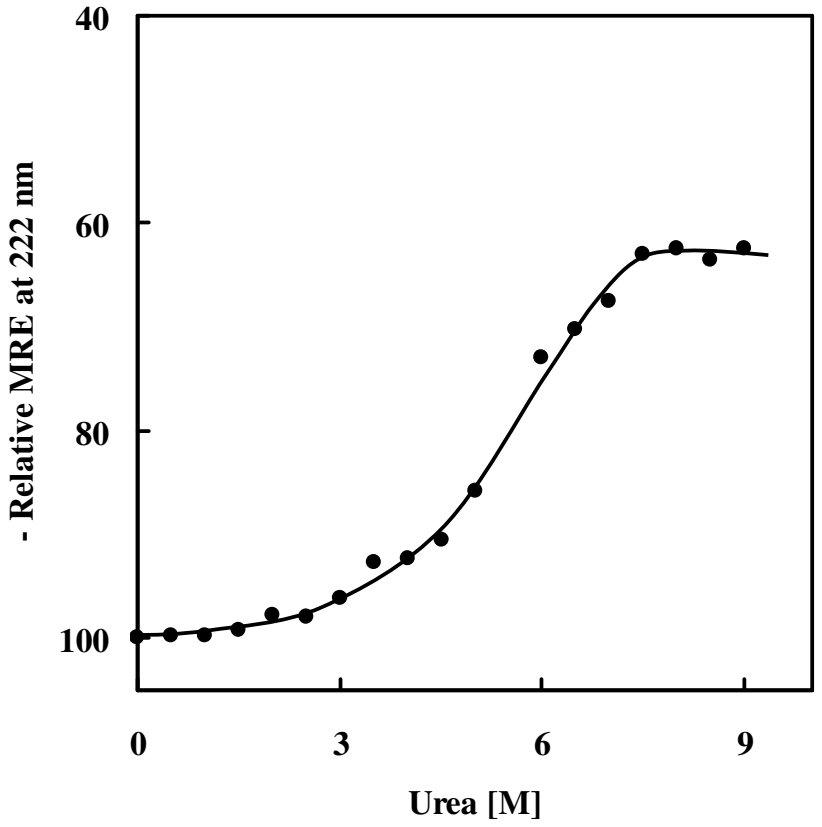

Figure 4.18: Plot of relative $MRE_{222\ nm}$ of S_{42} BLA in 0.02 M Tris-HCl buffer, pH 7.5 at 25°C versus urea concentration. Relative $MRE_{222\ nm}$ values at each urea concentration were calculated by taking the $MRE_{222\ nm}$ value of S_{42} BLA in the absence of urea as 100.

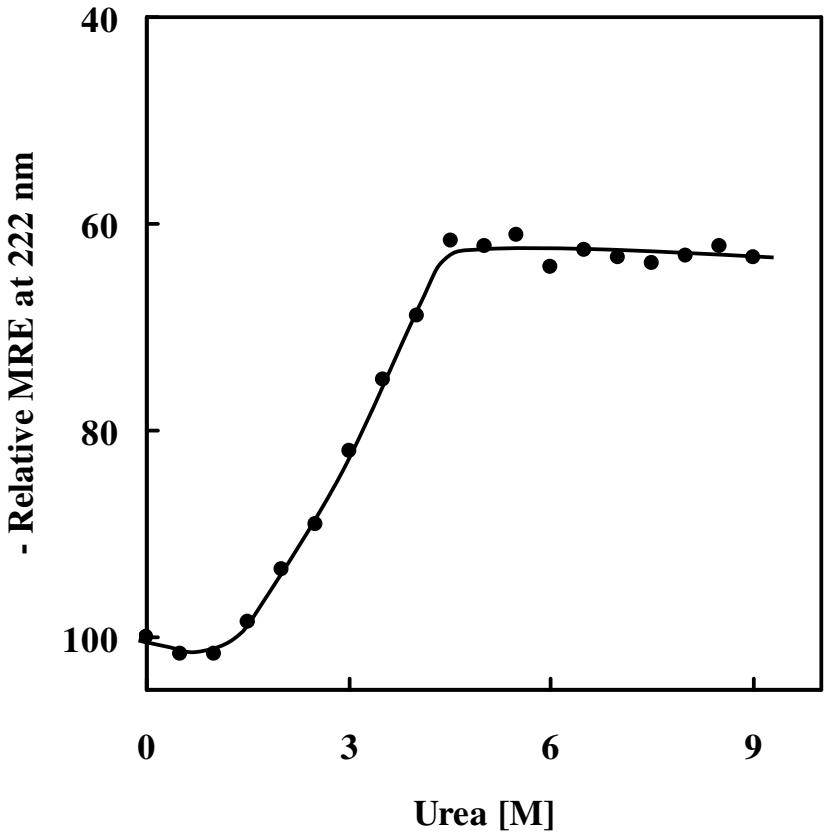

Figure 4.19: Plot of relative $MRE_{222\ nm}$ of C_{81} BLA in 0.02 M Tris-HCl buffer, pH 7.5 at 25°C versus urea concentration. Relative $MRE_{222\ nm}$ values at each urea concentration were calculated by taking the $MRE_{222\ nm}$ value of C_{81} BLA in the absence of urea as 100.

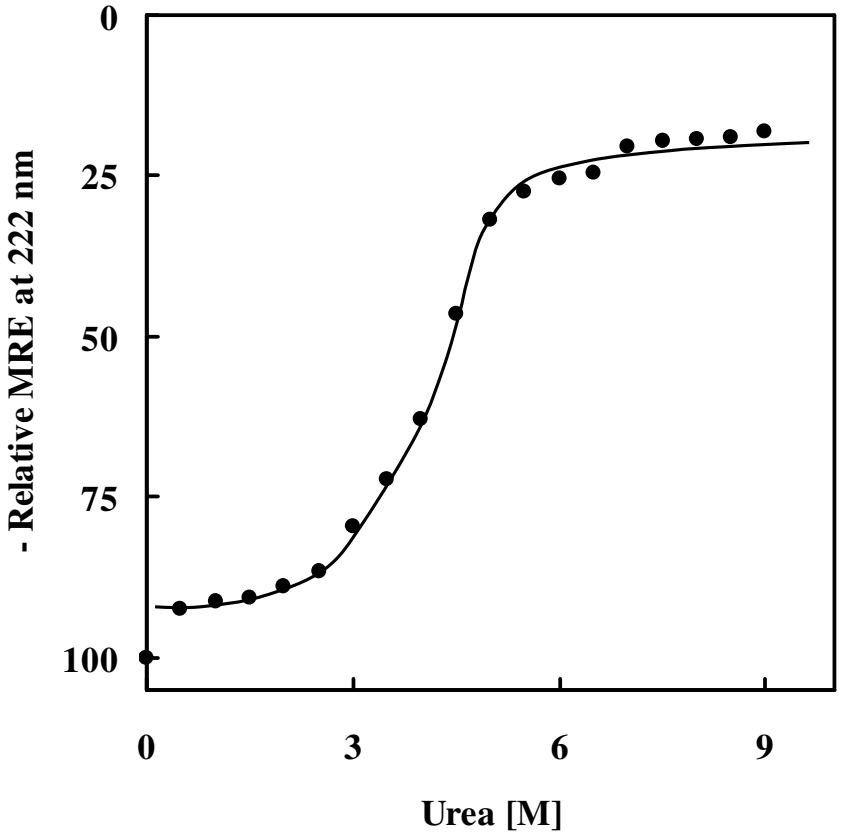

Figure 4.20: Plot of relative $MRE_{222\ nm}$ of G_{88} BLA in 0.02 M Tris-HCl buffer, pH 7.5 at 25°C versus urea concentration. Relative $MRE_{222\ nm}$ values at each urea concentration were calculated by taking the $MRE_{222\ nm}$ value of G_{88} BLA in the absence of urea as 100.

Urea denaturation data of native and modified BLA preparations were analyzed using a two-state model by converting $MRE_{222\ nm}$ values at each urea concentration into F_D (Fraction denatured) values as described in 'Materials and methods'. Figures 4.21A–4.25A show plots of F_D values against urea concentration for native, Ca-depleted, S_{42}, C_{81} and G_{88} BLA preparations respectively. It should be noted that values for start-, mid- and end-points of transitions remained the same as described above (Table 4.4). Values of F_D (falling in the range, 0.20–0.80) were transformed into K_D and subsequently into ΔG_D values at each urea concentration following standard procedures in order to quantify the loss in conformational stability of BLA induced by these modifications. Figures 4.21B–4.25B show corresponding linear plots of ΔG_D against urea concentration for native and modified preparations respectively. Values of free energy of stabilization ($\Delta G_D^{H_2O}$) for native and modified preparations were determined from the Y-axis intercept of these linear plots and are given in Table 4.4. Native BLA had a $\Delta G_D^{H_2O}$ value of 5,930 cal/mol whereas $\Delta G_D^{H_2O}$ value obtained with Ca-depleted BLA was found to be 3,430 cal/mol (Table 4.4). All modified preparations (S_{42}, C_{81} and G_{88} BLAs) also had lower $\Delta G_D^{H_2O}$ values *i.e.* 3,957, 3,336 and 3,383 cal/mol for S_{42}, C_{81} and G_{88} BLAs respectively (Table 4.4) compared to native BLA.

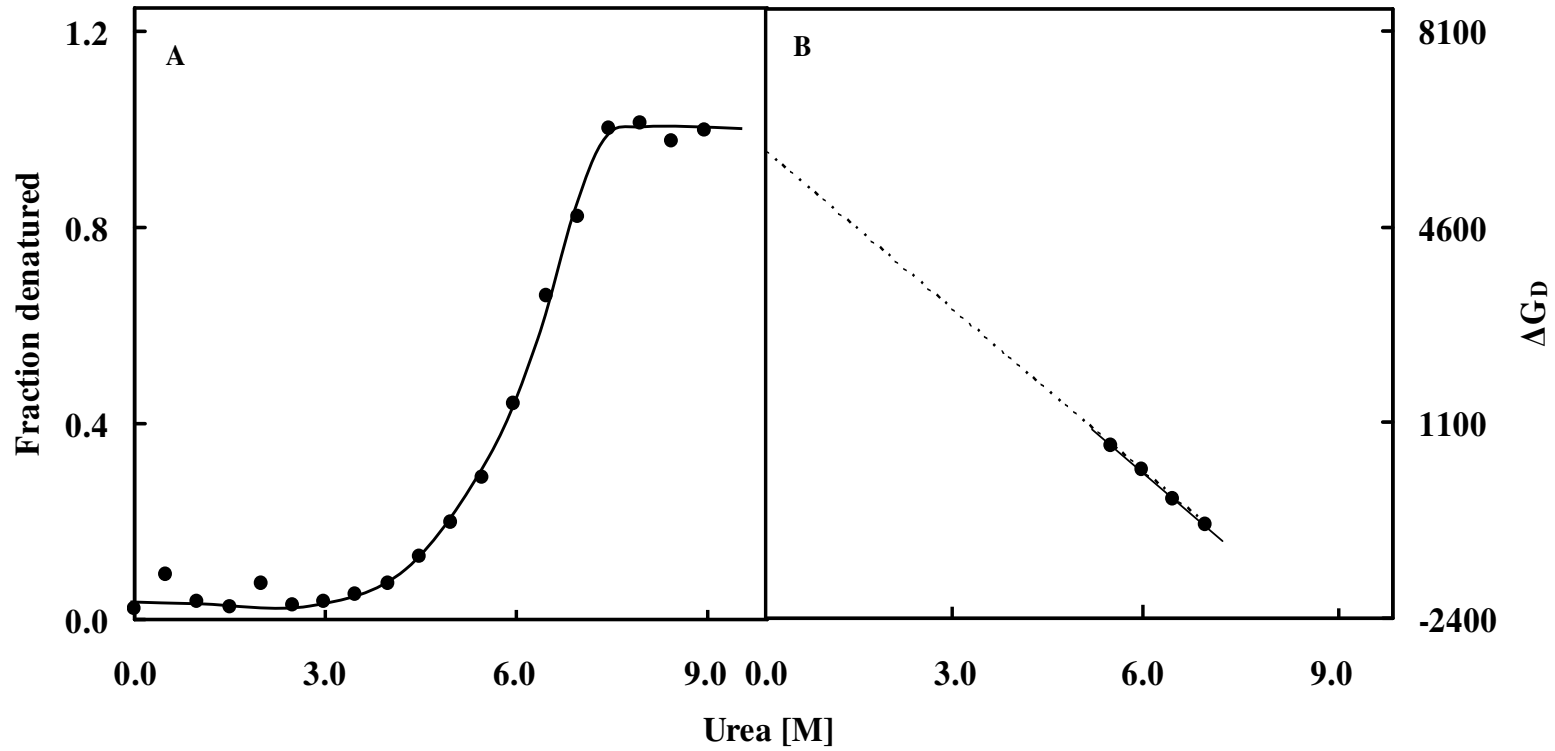

Figure 4.21: (A) Normalized transition curve for urea denaturation of native BLA in terms of F_D (Fraction denatured) versus urea concentration as followed by MRE measurements at pH 7.5, 25°C shown in Figure 4.16. (B) Plot of ΔG_D against urea concentration for the transition shown in (A).

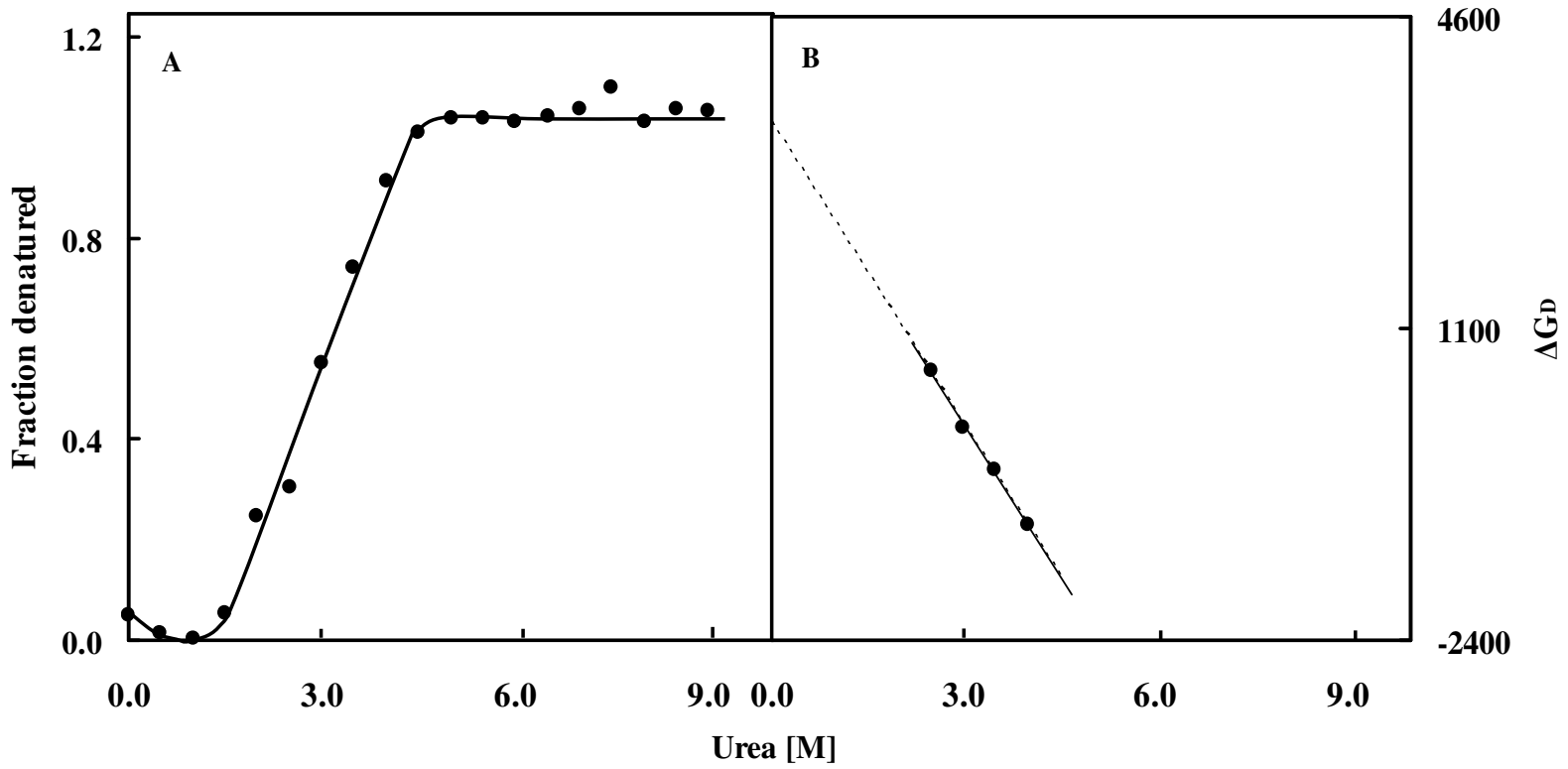

Figure 4.22: (A) Normalized transition curve for urea denaturation of Ca-depleted BLA in terms of F_D (Fraction denatured) versus urea concentration as followed by MRE measurements at pH 7.5, 25°C shown in Figure 4.17. (B) Plot of ΔG_D against urea concentration for the transition shown in (A).

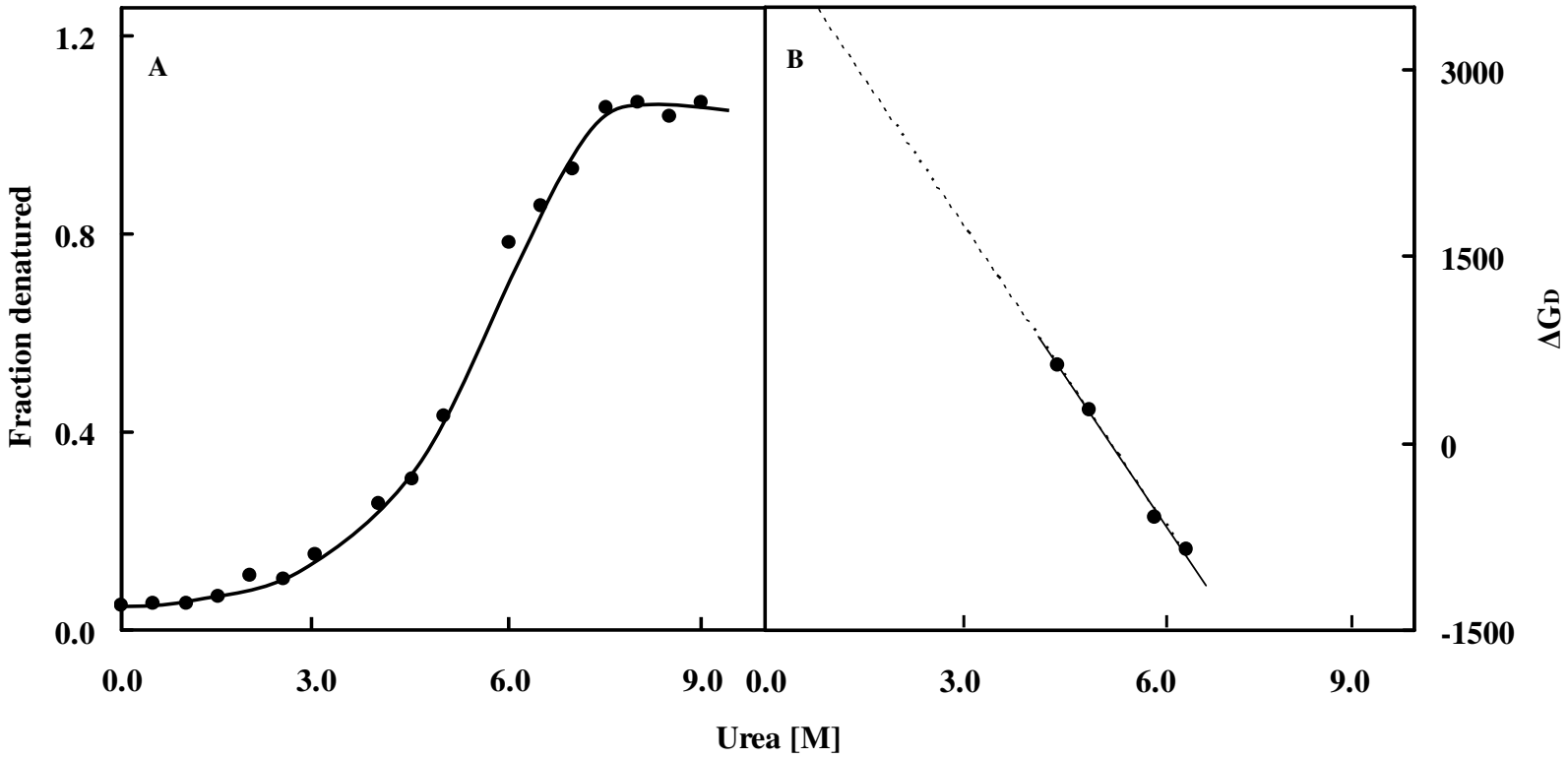

Figure 4.23: (A) Normalized transition curve for urea denaturation of S_{42} BLA in terms of F_D (Fraction denatured) versus urea concentration as followed by MRE measurements at pH 7.5, 25°C shown in Figure 4.18. (B) Plot of ΔG_D against urea concentration for the transition shown in (A).

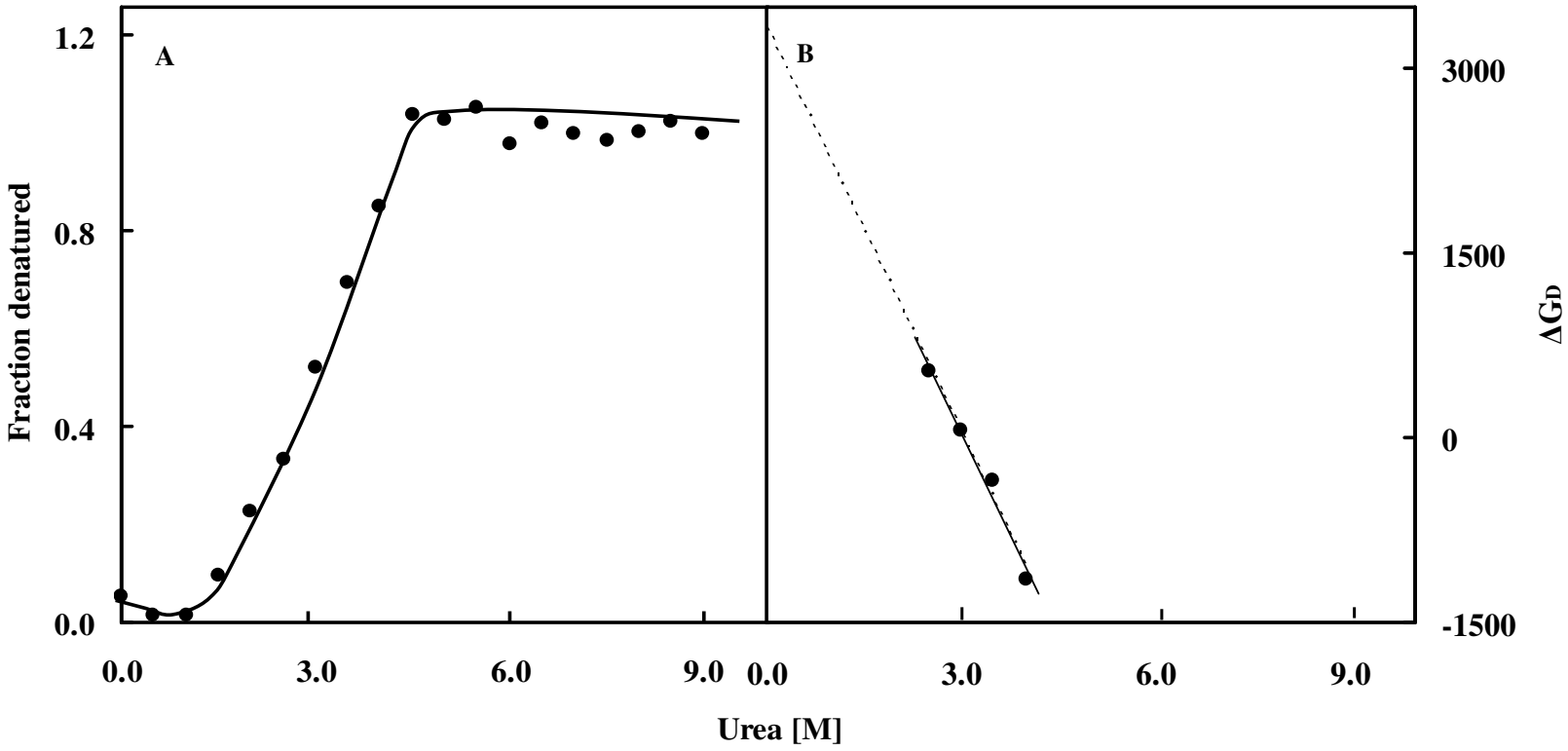

Figure 4.24: (A) Normalized transition curve for urea denaturation of C_{81} BLA in terms of F_D (Fraction denatured) versus urea concentration as followed by MRE measurements at pH 7.5, 25°C shown in Figure 4.19. (B) Plot of ΔG_D against urea concentration for the transition shown in (A).

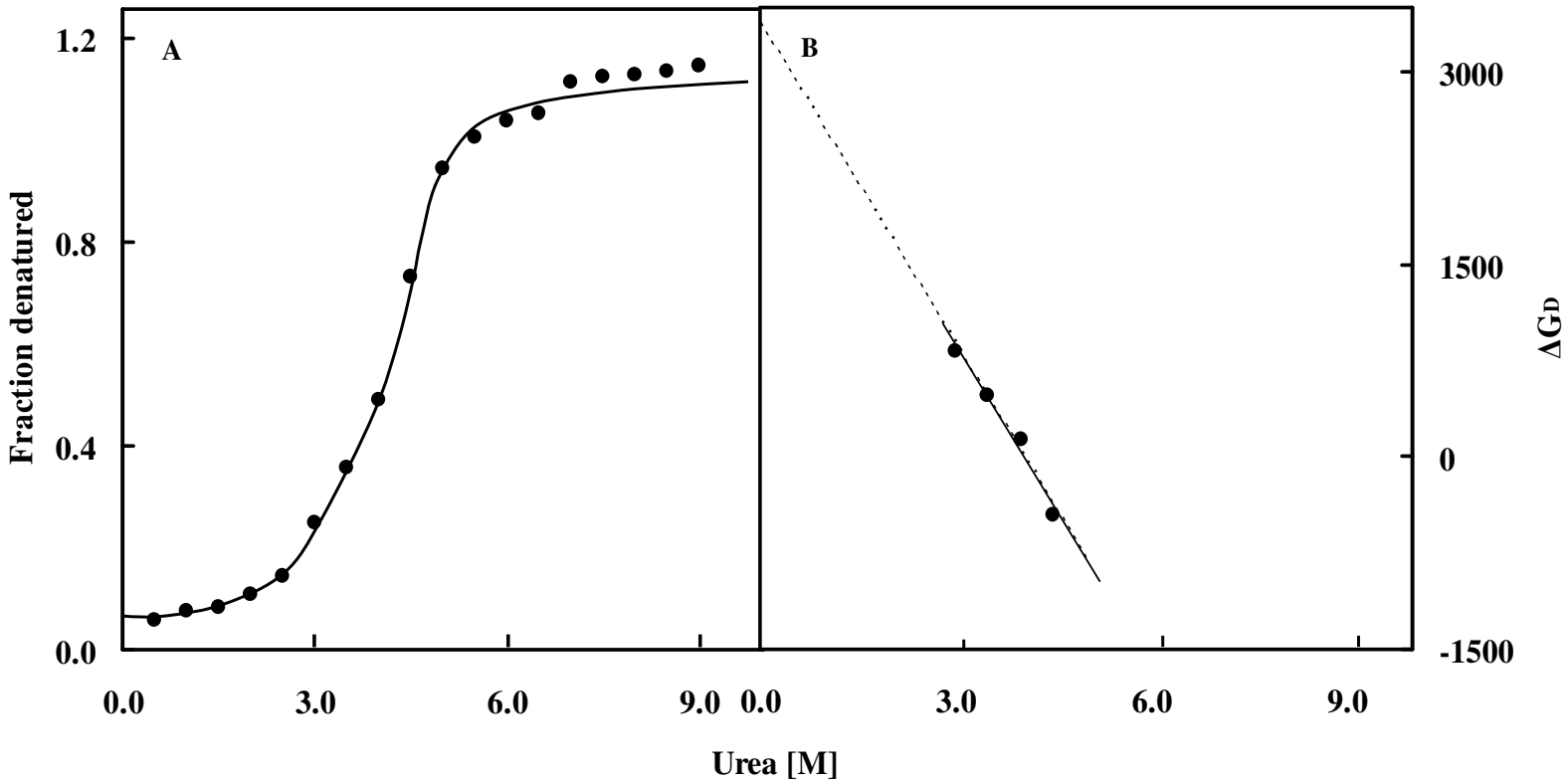

Figure 4.25: (A) Normalized transition curve for urea denaturation of G_{88} BLA in terms of F_D (Fraction denatured) versus urea concentration as followed by MRE measurements at pH 7.5, 25°C shown in Figure 4.20. (B) Plot of ΔG_D against urea concentration for the transition shown in (A).

CHAPTER 5

DISCUSSION

5.1 Effect of calcium on GdnHCl denaturation of native and Ca-depleted BLAs

5.1.1 Circular dichroism

Circular dichroism is a routine technique employed to follow the changes in the secondary structures of a protein. Typically, any difference in MRE at 222 nm is indicative of the change in the α-helical content of a protein. The significant decrease in MRE observed up to 3.5 M GdnHCl concentration (Figure 4.1) was suggestive of the unfolding of native BLA due to the loss in the α-helical content. Similar decrease in MRE with increasing GdnHCl concentrations has been reported for a number of proteins (Lai et al., 1997; Kumar et al., 2005; Usha & Ramasami, 2008). Significant precipitation below 2.0 M GdnHCl can be ascribed to strong aggregation and has also been observed in an earlier study (Strucksberg et al., 2007). The CD data beyond 3.5 M GdnHCl revealed unusual results. Although ~25% increase in MRE up to 6.0 M GdnHCl was suggestive of some reversal in the helical content of the protein, nevertheless MRE value at 6.0 M GdnHCl was still much lesser (~43%) than the MRE value of native BLA suggesting protein denaturation. Since only domain A out of the three domains of BLA contains eight α-helical segments of varying lengths (Machius et al., 1995), changes in MRE at different GdnHCl concentrations is primarily the reflection of structural changes in domain A of BLA. Presence of 2 mM $CaCl_2$ in the incubation mixture offered significant stability to native BLA against GdnHCl denaturation as reflected from the increase in MRE values throughout the GdnHCl concentration range (Figure 4.1). This seems understandable as calcium binding to the three calcium binding sites in BLA (partially saturated in commercial preparation) has been shown to offer structural integrity to the enzyme (Vihinen & Mäntsälä, 1989;

Violet & Meunier, 1989). Non-occurrence of the precipitation at lower GdnHCl concentrations (<2.0 M) in the presence of 2 mM $CaCl_2$ can possibly be explained by the stabilizing effect of calcium ions on BLA as well as promoting repulsion among unfolded enzyme molecules.

Native BLA does not represent a well-defined state of the protein as it might be partially saturated with calcium. In view of this, denaturation profile observed with native BLA in the absence of calcium as shown in Figure 4.1 may not represent the actual denaturation profile of the pure protein. Therefore, Ca-depleted BLA was prepared from native commercial preparation in order to get a clear understanding about its denaturation behaviour. A marked reduction in MRE (~74%) at 2.0 M GdnHCl observed with Ca-depleted BLA (Figure 4.2) against ~54% decrease seen with native BLA (Figure 4.1) suggested stabilization of native BLA by intrinsic calcium. This was further justified by the complete denaturation (~98% loss in MRE) of Ca-depleted BLA at 6.0 M GdnHCl (Figure 4.2) whereas native BLA still possessed ~55% MRE signal at the same GdnHCl concentration. Addition of 2 mM $CaCl_2$ in the incubation mixture stabilized the enzyme (Ca-depleted BLA) against GdnHCl denaturation in the range, 1.5–6.0 M. However, the reversal in MRE values was lesser (Figure 4.2) than the reversal observed with native BLA (Figure 4.1). Interestingly, values of MRE observed with Ca-depleted BLA in presence of 2 mM $CaCl_2$ were found comparable to those observed with native BLA in the absence of 2 mM $CaCl_2$. This signifies that addition of 2 mM $CaCl_2$ to Ca-depleted BLA was sufficient to confer same degree of stability to that exhibited by intrinsic calcium present in native BLA. Irrespective of the values of MRE obtained in presence of 2 mM $CaCl_2$ with both native and Ca-depleted BLAs, both preparations showed significant reversal in MRE at all the GdnHCl concentrations. This unequivocally showed the stability conferred by 2 mM $CaCl_2$ to BLA against

GdnHCl denaturation. In an earlier study, calcium has been shown to induce renaturation of urea-unfolded BLA (Nazmi et al., 2006).

5.1.2 Intrinsic fluorescence

In proteins, there are only three intrinsic fluorophores, namely Trp, tyrosine (Tyr) and phenylalanine (Phe) with larger to smaller quantum yield respectively (Lakowicz, 2006). In general, studies involving Trp fluorescence are practiced due to low quantum yield of Phe and quenching of Tyr fluorescence by neighbouring Trp residues. Being a class B protein (Weber, 1960) with 17 Trp residues (Duy & Fitter, 2006), fluorescence emission in BLA is solely attributed to Trp residues. Presence of emission maximum in the fluorescence spectra of both native and Ca-depleted BLAs at 336 and 338 nm respectively supported this fact. All 17 Trp residues of BLA are much more buried in the protein interior (Duy & Fitter, 2006). Fluorescence characteristics (fluorescence intensity and emission maximum) of a protein are sensitive to the environment around fluorophores. Decrease in fluorescence intensity and red shift in emission maximum can be ascribed to either the exposure of Trp residues to the solvent or change in microenvironment around Trp residues from nonpolar to polar (Svensson et al., 2003; Duy & Fitter, 2006). Therefore, it seems plausible to assume that decrease in relative fluorescence intensity up to 1.0 M GdnHCl concentration observed in both native and Ca-depleted BLAs was due to the exposure of buried Trp residues to the solvent, suggesting protein denaturation (Figures 4.3 and 4.4) (Singh & Bhakuni, 2009). However, the extent of denaturation was relatively higher in Ca-depleted BLA than native BLA which seems appropriate due to the stability conferred by intrinsic calcium to native BLA. Lack of protein precipitation at lower GdnHCl concentrations in fluorescence experiments can be explained by the lower protein concentration (0.1 μM) used compared to 1.8 μM used in CD experiments. On the other hand, the increase in

fluorescence intensity at higher GdnHCl concentrations (Figures 4.3 and 4.4) may be accounted for the formation of small hydrophobic loop-like structures surrounding Trp residues. This can be justified from the primary sequence of BLA where most of the neighboring residues around Trp are hydrophobic in nature (Declerck et al., 2002). Our emission maximum results of native and Ca-depleted BLAs (Figures 4.5 and 4.6) also support this contention, where the occurrence of red shift indicating exposure of Trp residues at initial GdnHCl concentrations and resurgence of emission maximum close to native BLA at higher GdnHCl concentrations were noticed. A continuous red shift in the emission maximum of native and Ca-depleted BLAs up to 3.0 M GdnHCl was in accordance with our CD data on native BLA (Figure 4.1). Presence of 2 mM $CaCl_2$ significantly reduced the changes in fluorescence intensity and emission maximum of both native and Ca-depleted BLAs, being more effective in native BLA showing stabilizing potential of calcium ions on native protein conformation against GdnHCl denaturation. Absence of any significant change in fluorescence signals (fluorescence intensity and emission maximum) of native BLA in presence of 2 mM $CaCl_2$ should not be taken as complete stabilization of native BLA against GdnHCl denaturation as significant secondary structural changes have been noticed under those conditions (Figure 4.1). Both fluorescence signals are sensitive to many conditions and the observed emission spectrum is the result of multiple conditions of five spectral classes (Duy & Fitter, 2006).

5.1.3 Enzymatic activity

The initial loss (~85%) in biological activity of native BLA observed at 1.0 M GdnHCl followed by gradual increment within 3.0–6.0 M GdnHCl concentration range (Figure 4.7) was similar to the pattern of MRE data of native BLA in the absence of 2 mM $CaCl_2$ (Figure 4.1). On the other hand, Ca-depleted BLA exhibited total loss in activity

at ≥ 1.0 M GdnHCl in the absence of 2 mM $CaCl_2$. In other words, removal of intrinsic calcium from BLA completely abolished the enzyme's ability to degrade starch even at lower GdnHCl concentrations. This was in accordance with an earlier study on Ca-depleted BLA (Strucksberg et al., 2007). Greater retention of enzymatic activity in both native and Ca-depleted BLAs at different GdnHCl concentrations but in presence of 2 mM $CaCl_2$ (Figures 4.7 and 4.8) can be explained on the basis of stabilizing potential of calcium on its structure. In view of the incomplete saturation of calcium binding sites of BLA in solutions (Nazmi et al., 2006), addition of 2 mM $CaCl_2$ into the buffer system might have increased calcium binding to the native enzyme. This in turn might have enhanced substrate binding due to the induction of ordered conformation of BLA resulting in the extension of substrate binding site (Machius et al., 1998). In an earlier study (Nazmi et al. 2006), native BLA was shown to retain substantial amount of secondary structure even at highest urea concentration and this behavior was attributed to the presence of calcium in native BLA. A similar calcium-induced stabilizing effect can be speculated for GdnHCl denaturation of native BLA. These factors might be responsible for the higher activity of native BLA in the presence of 2 mM $CaCl_2$. This explanation seems to be justified from our results on Ca-depleted BLA (devoid of intrinsic calcium) where absence of 2 mM $CaCl_2$ rendered the enzyme labile towards GdnHCl denaturation leading to complete loss of biological activity (Figure 4.8). Addition of 2 mM $CaCl_2$ in the incubation mixture offered some stability to both enzyme forms resulting in enhancement of enzymatic activity. A comparison of the structures of native and Ca-depleted forms of BLA showed differences in the structures of holo- and apo-enzymes (Machius et al., 1998). The segment between residues 182 and 192 containing the metals' ligand and essential *cis* peptide bond was found to be completely disordered in the apo form. This structural difference between native and

Ca-depleted BLAs could possibly account for the difference in the biological activity of these states.

5.2 Chemical modifications of lysine residues of BLA

Formation of yellow colored trinitrophenyl derivatives with an absorption maximum at 335 nm in TNBSA reaction with proteins was employed to quantify the modification of lysine residues in BLA (Habeeb, 1966). Since TNBSA reacts with amino groups (α-amino and ε-amino) of proteins, any reduction in the color intensity can be attributed to the modification of amino groups of proteins. Decrease in the slope value of the plot between absorbance at 335 nm versus amount of protein observed with BLA preparations treated with different modifying agents (Table 4.1) was suggestive of the modification of lysine residues in these preparations. A total of 12, 24 and 26 amino groups were found to be modified in 42% succinylated (S_{42}), 81% carbamylated (C_{81}) and 88% guanidinated (G_{88}) BLAs respectively by taking the total number of amino groups in BLA as 29 (1 α-amino + 28 ε-amino) (Tomazic & Klibanov, 1988).

Emergence of single band for each preparation in electrophoretogram was indicative of charge homogeneity of all BLA preparations. Increased anodic mobilities (0.47) of both S_{42} and C_{81} BLA preparations compared to 0.09 obtained with native BLA (Table 4.1) was in accordance with the increase in the net negative charge of these preparations. In view of the isoelectric point of native BLA as 6.0 (Shaw et al., 2008), the net charge on the protein would be negative at pH 8.3 (reaction condition for PAGE), which can account for the anodic mobility of native BLA. Since succinylation increases the net negative charge on the protein by 2 units per lysine residue modified against the increase of 1 unit in carbamylation reaction, succinylated preparation would have more net negative charge compared to carbamylated derivative. However, extent of

modification in succinylated preparation was about half of that obtained with C_{81} BLA thus, the net negative charge in both these preparations would have been similar but higher than native BLA which can account for the same but higher relative mobility observed with these preparations. On the other hand, G_{88} BLA preparation showed lesser deviation (0.06) compared to the relative mobility of native BLA. This can be explained by the retention of positive charge on modified lysine residues hence, no alteration of anodic movement in PAGE. Size homogeneity of native and modified BLA preparations was evident from their elution profiles (Figures 4.11–4.13) on Sephacryl S-200 HR column (1.63×56 cm) in which each preparation eluted in the form of single symmetrical peak. Trailing in the ascending limb of the elution profile of G_{88} BLA might represent the presence of some aggregates in this preparation which seems possible due to increased hydrophobicity of homoarginine residues (in G_{88} BLA) formed as a result of guanidination reaction (Chiti et al., 2003; Shaw et al., 2008).

5.3 Conformational changes in modified BLAs

Conformational changes in all modified preparations were evident from the change in their elution volumes compared to native BLA on Sephacryl S-200 HR column (1.63 × 56 cm). Elution volume being inversely correlated with the molecular size of the protein (Andrews, 1970), decrease in elution volume of S_{42} (65.0 ml) and C_{81} (63.0 ml) BLAs against 89.0 ml obtained with native BLA (Table 4.2) were indicative of the increase in their hydrodynamic volumes whereas increase in elution volume (110.0 ml) of G_{88} BLA suggested a decrease in its molecular size. The effect of succinylation, carbamylation and guanidination on the conformation of BLA was further verified from their Stokes radii values (Table 4.3). The Stokes radius of native BLA (2.43 nm) as obtained from gel chromatographic data was lower than the value (3.20 nm) determined from dynamic light scattering (Fitter & Haber-Pohlmeier, 2004). Such anomalous behavior of BLA on

gel chromatographic column was not surprising as interaction of α-amylases with various gel matrices have been reported earlier (Kruger & Lineback, 1987). Irrespective of this anomalous behavior, useful information about the change in hydrodynamic volume can be obtained by comparing the Stokes radii (determined from analytical gel chromatography) of modified proteins to their native form.

Both succinylated and carbamylated BLA preparations had higher Stokes radii than their native counterpart (Table 4.3). Furthermore, C_{81} BLA showed relatively higher Stokes radius (3.40 nm) than S_{42} BLA (3.34 nm) which seemed appropriate in view of the higher extent of modification in carbamylated preparation. The increase in hydrodynamic volume of BLA upon succinylation and carbamylation was in agreement with several previous reports suggesting succinylation- and carbamylation-induced conformational changes in proteins (Habeeb, 1967; Beswick & Harding, 1984; Qin et al., 1992; Tayyab et al., 1999; Khan & Tayyab, 2001; Derham & Harding, 2002). In view of the increase in net negative charge on the protein by 2 and 1 units in succinylation and carbamylation reactions respectively per lysine residue modified, both succinylated and carbamylated BLAs would have higher electrostatic free energy than native BLA which was responsible for their conformational destabilization. Although the increase in net negative charge on S_{42} and C_{81} BLAs would be the same ($2\times12 = 24$ in S_{42} BLA and $1\times24 = 24$ in C_{81} BLA), conformational alteration observed in C_{81} BLA was slightly higher than S_{42} BLA. This is because only 12 amino groups were modified in S_{42} BLA against 24 amino groups modified in C_{81} BLA. In other words, C_{81} BLA had both surface-exposed and partially buried lysine residues modified compared to the modification of only surface-exposed lysine residues in S_{42} BLA. Modification of these partially buried lysine residues would have destabilized the native conformation more intensely in C_{81} BLA compared to the modification of surface-exposed lysine residues

in S_{42} BLA. On the other hand, decrease in Stokes radius of G_{88} BLA (1.76 nm) was suggestive of a more compact conformation in G_{88} BLA. Although this is not an unusual observation as guanidination of several proteins has been shown to induce more compact conformation than their native counterparts (Spero et al., 1971; Mita et al., 1981; Tayyab et al., 1999), nonetheless the significant difference in the Stokes radius of G_{88} BLA from its native protein could partially be attributed to the possible interaction(s) between G_{88} BLA and the gel matrix (Spero et al., 1971).

5.4 Conformational stabilities of native, Ca-depleted and modified BLAs

To investigate the effect of chemical modification on the conformational stability of native BLA, urea denaturation of native BLA and its modified derivatives was studied in 0.02 M Tris-HCl buffer, pH 7.5 using CD spectral signal in the far-UV range (MRE at 222 nm). Since BLA contains three calcium binding sites (Machius et al., 1998) and bound calcium has been shown to offer structural stability to the enzyme in several earlier reports (Vihinen & Mäntsälä, 1989; Violet & Meunier, 1989) as well as in this study, we thought it of interest to study the conformational stability of commercially available BLA (partially saturated with calcium) both before and after calcium depletion using urea denaturation.

The urea transition curve of Ca-depleted BLA (Figure 4.17) was in agreement both in terms of the start point and the percentage decrease of MRE at the completion of transition with the only report available on urea denaturation of Ca-depleted BLA (Nazmi et al., 2006). However, both mid- and end-points of the transition observed in this study were slightly higher than the reported values. These differences might be due to different reaction conditions employed in these studies (pH 8.0 and 20°C versus pH 7.5 and 25°C). The shift observed in the whole transition curve of native BLA (partially

saturated with calcium) towards higher urea concentration was suggestive of higher stability of native BLA against urea denaturation compared to Ca-depleted BLA. Such higher stability can be ascribed to the presence of bound calcium in native BLA. The requirement of calcium for maintaining the structural integrity of BLA has also been suggested earlier (Vihinen & Mäntsälä, 1989; Violet & Meunier, 1989; Feller et al., 1999). However, the decrease in MRE value at the completion of the transition of native BLA was only 55% (Figure 4.16) which was 28% lesser than the decrease observed with Ca-depleted BLA (Figure 4.17). Decrease in MRE value at 222 nm is indicative of the loss of α-helical content in proteins (Du & Wang, 2003; Naoe et al., 2004). In view of this, lesser decrease in $MRE_{222\ nm}$ in native BLA at the completion of transition suggested retention of some α-helical structures, stabilized by bound calcium. This seems possible as all the three calcium binding sites involve some contribution from domain A which contains all the 8 segments of α-helices available in BLA (Machius et al., 1998).

In an earlier study (Nazmi et al., 2006), native BLA has been reported to be resistant against urea denaturation even though a ~25% decrease in MRE was observed at the highest urea concentration. However, we noticed a cooperative urea transition in native BLA with a 55% decrease in MRE at the completion of transition (Figure 4.16). A smaller change in MRE (~25%) observed in an earlier study (Nazmi et al., 2006), compared to 55% shown in this study can be attributed to the different amount of bound calcium available in these preparations which provides stability to different extent against urea denaturation (Kumari et al., 2010). This seems understandable as these preparations were obtained from different companies (Novozymes and Sigma) which might have used different enzyme purification strategies. Furthermore, this can be justified by our urea denaturation results on Ca-depleted BLA in presence of 2 mM

$CaCl_2$ (Figure 4.17) where the onset of transition was delayed at 2.5 M urea (against 1.0 M in the absence of 2 mM $CaCl_2$) and ~30% decrease in MRE was noted at the highest urea concentration compared to 83% observed with the same preparation but in the absence of 2 mM $CaCl_2$. This was further supported by our results on urea denaturation of native BLA in presence of 2 mM $CaCl_2$ where the enzyme was found to be completely resistant towards urea denaturation as reflected from the unfluctuating MRE values throughout the urea concentration range. In view of this, 25% change in MRE of native BLA shown in an earlier study (Nazmi et al., 2006) suggested presence of greater amount of bound calcium in their preparation. Taken together, a comparison of urea transition curves obtained with Ca-depleted and native BLAs, both in the absence and presence of 2 mM $CaCl_2$ suggested stabilizing effect of calcium towards urea denaturation of BLA.

Since all modified preparations (S_{42}, C_{81} and G_{88} BLAs) were prepared from native BLA, it would be logical to compare their transition curves (Figures 4.18–4.20) with the transition curve obtained with native BLA (Figure 4.16). A comparison of these BLA preparations (native, S_{42}, C_{81} and G_{88} BLAs) revealed a shift in the transition curve towards the left side (lower urea concentrations) in all modified preparations suggesting lower conformational stability of these preparations which was more pronounced with C_{81} and G_{88} BLAs compared to S_{42} BLA (Table 4.4). In view of the modification of 11 and 23 out of 28 lysine residues in S_{42} and C_{81} BLA preparations respectively, a relatively lower stability of C_{81} BLA is justifiable as it might contained some modified buried lysine residues as well. Interestingly, urea transition characteristics of C_{81} BLA matched very well with the transition characteristics of Ca-depleted BLA. In other words, conformational stabilities of C_{81} BLA and Ca-depleted BLA seem to be similar which was also evident from the similar values of $\Delta G_D^{H_2O}$ (Table 4.4).

Considering the location of three calcium binding sites in BLA (two in domain B and one at the interface between domains A and C) with high negative charge density particularly around the two binding sites in domain B (Machius et al., 1998), it seems likely that modification of lysine residues in C_{81} preparation might have disrupted the charge balance in domain B and at the interface of domains A and C leading to the release of calcium from the metal binding sites in this preparation. In an earlier report, presence of a *cis* peptide bond between Trp 184 and Glu 185 has been suggested to be important for maintaining the correct structure of metal binding site in domain B. Lys 276 has also been proposed to stabilize the *cis* peptide bond conformation through ionic interaction with Glu 185 (Machius et al., 1998). It appears likely that C_{81} BLA might have Lys 276 modified resulting in the derangement of the calcium binding site. Together, both these explanations seem to be in favor of the disruption of the calcium binding site in C_{81} BLA which might be responsible for the release of calcium leading to similarity in urea transition curve of C_{81} BLA with that of Ca-depleted BLA. Furthermore, a significant proportion of known (14) ionic interactions involving Lys residues in BLA (Machius et al., 1995) might have been disrupted in C_{81} BLA, producing gross conformational changes and thus destabilized the enzyme. Absence of such phenomenon in S_{42} BLA can be explained on the basis of lesser extent of modification which might have not modified the critical lysine residue(s) responsible for the stability of calcium binding site(s). Our gel chromatographic data supported this contention as C_{81} BLA showed larger conformational change compared to S_{42} BLA (Table 4.3). Lesser decrease in MRE observed with both modified preparations at the completion of transition may be the result of the loss of asymmetric environment of aromatic amino acid residues at higher urea concentration in these preparations (Boren et al., 1999).

The transition characteristics of G_{88} BLA preparation had fallen in between the transition characteristics of native and Ca-depleted BLAs (Table 4.4) suggesting similarity of this preparation to Ca-depleted BLA with respect to the start of the transition while retaining features of stability in terms of the mid- and end-points of the transition. Although G_{88} BLA showed a more compact conformation than native BLA due to the increase in hydrophobicity, possibility of the loss of calcium from calcium binding sites in BLA cannot be ruled out in G_{88} BLA preparation. A partial but not the complete loss of intrinsic calcium can probably explain the falling of mid- and end-point characteristics of G_{88} BLA in between native and Ca-depleted BLAs (Table 4.4). In view of this, it is conceivable to think of the retention of intermediate stability in G_{88} BLA compared to those of native and Ca-depleted BLAs. Since the presence of calcium adds more to the stability of BLA (Vihinen & Mäntsälä, 1989; Violet & Meunier, 1989; Feller et al., 1999), the decrease in $\Delta G_D^{H_2O}$ and other transition characteristics in G_{88} BLA cannot be taken as the destabilization of native protein conformation upon guanidination. Therefore, these results are in line of earlier observation on guanidination suggesting more or less similar stability of guanidinated preparations (Cupo et al., 1980; Tayyab et al., 1999; Shibuya et al., 1982).

CHAPTER 6

CONCLUSION

Calcium was found to stabilize both native and Ca-depleted BLAs against urea and GdnHCl denaturations as judged by significantly lesser changes in mean residue ellipticity, fluorescence intensity, emission maximum and biological activity of these enzymes in presence of 2 mM $CaCl_2$ compared to those observed in its absence.

Lysine residues of BLA were found to play an important role in the conformational stability of the enzyme as modification of lysine residues decreased the free energy of stabilization of BLA. This decrease in conformational stability can be ascribed to the significant conformational changes occurred in the enzyme upon modification leading to the release of intrinsic calcium from calcium binding sites. Therefore, lysine residues are essential in maintaining the native structure of the enzyme through electrostatic interactions.